Development of Metastable Processing Paths

for

High Temperature Alloys

Semi-Annual Technical Report
submitted to
Defense Advanced Research Projects Agency (DoD)
for the period
October 1, 1988 through March 31, 1989

Contractor: Metallurgy Division
National Institute of Standards and Technology
Gaithersburg, MD 20899

Principal Investigator: William J. Boettinger
301-975-6160

Senior Project Scientists: Leonid A. Bendersky
John W. Cahn
Ursula R. Kattner

Effective Date of Contract: February 9, 1987

Contract Expiration Date: December 31, 1989

Amount of Contract: $600,000

ARPA Order Number: 6065

Program Code Number: 7D10

UNCLASSIFIED

SECURITY CLASSIFICATION OF THIS PAGE

REPORT DOCUMENTATION PAGE				Form Approved OMB No. 0704-0188
1a. REPORT SECURITY CLASSIFICATION UNCLASSIFIED			1b. RESTRICTIVE MARKINGS None	
2a. SECURITY CLASSIFICATION AUTHORITY N/A			3. DISTRIBUTION/AVAILABILITY OF REPORT Approved for Public Release Distribution Unlimited	
2b. DECLASSIFICATION/DOWNGRADING SCHEDULE N/A				
4. PERFORMING ORGANIZATION REPORT NUMBER(S) N/A			5. MONITORING ORGANIZATION REPORT NUMBER(S)	
6a. NAME OF PERFORMING ORGANIZATION Metallurgy Div., NIST	6b. OFFICE SYMBOL (If applicable) 450		7a. NAME OF MONITORING ORGANIZATION	
6c. ADDRESS (City, State, and ZIP Code) Gaithersburg, MD 20899			7b. ADDRESS (City, State, and ZIP Code)	
8a. NAME OF FUNDING/SPONSORING ORGANIZATION DARPA	8b. OFFICE SYMBOL (If applicable)		9. PROCUREMENT INSTRUMENT IDENTIFICATION NUMBER	
8c. ADDRESS (City, State, and ZIP Code)			10. SOURCE OF FUNDING NOS.	
			PROGRAM ELEMENT NO.	PROJECT NO. / TASK NO. / WORK UNIT ACCESSION NO.

11. TITLE (Include Security Classification)
Development of Metastable Processing Paths for High Temperature Alloys

12. PERSONAL AUTHOR(S)
W.J. Boettinger, L.A. Bendersky, J.W. Cahn, and U.R. Kattner

13a. TYPE OF REPORT	13b. TIME COVERED	14. DATE OF REPORT (Year, Month, Day)	15. PAGE COUNT
Semi-Annual Technical	FROM 10/1/88 TO 3/31/89	May 23, 1989	62

16. SUPPLEMENTARY NOTATION

17. COSATI CODES			18. SUBJECT TERMS (Continue on reverse if necessary and identify by block number)
FIELD	GROUP	SUB. GR.	Intermetallics, Ti/Nb Aluminides, Phase Diagram, Rapid Solidification, Ternary Alloys, Solid State Quenching

19. ABSTRACT (Continue on reverse if necessary and identify by block number)

This report describes research to: (a) develop predictive models for solubility extension and metastable phase formation of intermetallic compounds by rapid solidification, (b) analyze the kinetics of decomposition of metastable phases involving ordering and (c) improve the phase diagram modeling of systems involving ordered phases.

Rapid solidification studies on the intermetallic system, NiAl-NiTi, using laser surface melting with examination by transmission electron microscopy has shown the suppression of the equilibrium intermediate Heusler phase, Ni_2AlTi, and extension of the composition range of the NiAl and NiTi phases. High temperature x-ray studies have been started to determine the equilibrium order at the solidus to form a basis for comparison to the order trapping theory (developed in previous reports).

20. DISTRIBUTION/AVAILABILITY OF ABSTRACT	21. ABSTRACT SECURITY CLASSIFICATION
☐ UNCLASSIFIED/UNLIMITED ☐ SAME AS RPT. ☐ DTIC USERS	UNCLASSIFIED

22a. NAME OF RESPONSIBLE INDIVIDUAL	22b. TELEPHONE (Include Area Code)	22c. OFFICE SYMBOL
W.J. Boettinger	301-975-6160	450

DD Form 1473, JUN 86 *Previous editions are obsolete.* UNCLASSIFIED

SECURITY CLASSIFICATION OF THIS PAGE

Development of Metastable Processing Paths

for

High Temperature Alloys

Semi-Annual Technical Report
submitted to
Defense Advanced Research Projects Agency (DoD)
for the period
October 1, 1988 through March 31, 1989

Contractor: Metallurgy Division
National Institute of Standards and Technology
Gaithersburg, MD 20899

Principal Investigator: William J. Boettinger
301-975-6160

Senior Project Scientists: Leonid A. Bendersky
John W. Cahn
Ursula R. Kattner

Effective Date of Contract: February 9, 1987

Contract Expiration Date: December 31, 1989

Amount of Contract: $600,000

ARPA Order Number: 6065

Program Code Number: 7D10

Table of Contents

Summary

The development of acceptable toughness and creep strength in high temperature intermetallic alloys is closely related to the formation of proper distributions of second phase particles. Phases are needed both to arrest crack growth at low temperatures and to resist creep at high temperatures. The possibility of developing new processing strategies for high temperature intermetallic compounds is being investigated. In particular rapid solidification and/or rapid solid state quenching followed by controlled heat treatment may provide new and unusual microstructures of multiphase materials. This report describes research performed in the Metallurgy Division at NIST to: (a) develop predictive models for solubility extension and metastable phase formation of intermetallic compounds by rapid solidification, (b) analyze the kinetics of decomposition of metastable phases involving ordering and (c) improve the phase diagram modeling of systems involving ordered phases.

In past reports, theory has been developed to predict the formation of the disordered form of intermetallic compounds during rapid solidification (disorder trapping). Using a modification of the Aziz solute trapping theory, solidification velocities have been determined to form, for example, a BCC phase from the melt when a B2 phase is the stable phase or a FCC phase when a $L1_0$ phase is the stable phase.

Rapid solidification studies on the intermetallic system, NiAl-NiTi, using laser surface melting with examination by transmission electron microscopy has shown the suppression of the equilibrium intermediate Heusler phase, Ni_2AlTi, and extension of the composition range of the NiAl and NiTi phases. High temperature x-ray studies have been started to determine the

equilibrium order at the solidus to form a basis for comparison to the order trapping theory.

Experimental work on ternary alloys surrounding the composition Ti_2NbAl to determine the phases present at equilibrium and develop an understanding of solid state phase transformations in this system has continued. TEM investigations are required to sort out the complex ordering reactions in this important alloy system. Previous reports documented the existence of a broad B2 region at high temperature. Research is now focussed on the transformations which occur when this B2 phase is quenched at different rates or heat treated at low temperatures. In depth results for an alloy midway between TiAl and Ti_2AlNb (Ti_4Al_3Nb) are reported here and show the formation of ω-type phases which transform at low temperature to a $B8_2$ phase.

With the goal of providing a thermodynamic calculation of the Ti-Al-Nb and Nb-Al-Si ternary phase diagrams using the THERMOCALC code which is consistent with experimental data collected at NIST and at U. Wisconsin (Ti-Al-Nb) and at UCSB (Nb-Al-Si) under a DARPA URI program, it was found necessary to refine the calculation of the Nb-Al and Nb-Si binary diagrams. A complete reevaluation of the binary data and calculation of phase boundaries has been completed.

I. Introduction

The development of high temperature materials is closely related to the formulation of processing strategies for chemically ordered phases. Most intermetallic compounds including aluminides, carbides, and silicides as well as high temperature ceramic phases are ordered. However, optimum mechanical properties are likely to come from intimate dispersions of several phases, some of which are ordered. These dispersions can be produced by a phase transformation sequence involving both ordering and phase separation beginning with a solid phase of a carefully selected unstable composition made by rapid solidification.

Recently, significant advances have occurred in the utilization and understanding of rapid solidification processing of alloys. Factors which promote refined segregation, solubility extension and metastable phase formation have been identified. However, much of this research has been focused towards disordered crystalline phases: i.e., terminal solid solutions, not ordered intermetallic compounds.

At the same time, significant advances have been realized in the thermodynamics and kinetics of order-disorder transitions. The distinction between first and higher order transitions has been clarified, the kinetics of ordering reactions and the structure and mobility of APB's have been determined and reactions that involve fine scale ordering and compositional separation have been studied.

This research attempts to combine the advances in these areas to develop new processing strategies for high temperature ordered multiphase materials.

In section II of this report we describe experimental research focused on determining the possibility of extending the solubility range of ordered phases by rapid solidification. Subsequent heat treatment of these metastable alloys can form stable high temperature multiphase mixtures. This research also includes an examination of the state of nonequilibrium order of rapidly quenched intermetallic compounds.

Section III of this report summarizes research at phase identification and solid state transformation in compositions surrounding Ti_2NbAl.

Section IV of this report describes phase diagram activities involving ordered phases. A complete reevaluation and calculation of the Nb-Al binary and Nb-Si diagrams have been produced. This is necessary to obtain a better thermodynamic calculation of the Ti-Al-Nb and Nb-Al-Si diagrams.

Section V of this report consists of preprints submitted for publication: "Omega-related Phases in a Ti-Al-Nb Alloy," Proceedings of the 47th Annual Meeting of the Electron Microscopy Society of America, and "Investigation of B2 and Related Phases in the Ti-Al-Nb System," Mat. Res. Soc. Symp. Proc.

II. Solubility Extension and Disordering of Intermetallic Compounds by Rapid Solidification - NiAl-NiTi Alloys

As a conclusion of research previously reported, a manuscript "Theory for the Trapping of Disorder and Solute in Intermetallic Phases by Rapid Solidification" by W. J. Boettinger and M. J. Aziz has been accepted by Acta Metallurgica.

Experimental research on the microstructure of rapidly solidified alloys in the NiAl-NiTi system has continued in collaboration with Professor Mike Aziz of Harvard using pico-second pulse melting. This technique produces solidification rates of 1-5 m/s. Results on alloys with composition Ni_2TiAl show that extremely fine $L2_1$ domains are produced by this technique suggesting that the solidification process produced the B2 phase with subsequent solid state ordering to the $L2_1$ structure. To be certain that a nonequilibrium solidification product was obtained, it is necessary to establish that the $L2_1$ phase exists up to the solidus. Although this is widely accepted in this system, it has never been determined directly. For this purpose we have initiated high temperature X-ray diffraction of Ni_2TiAl to measure the long range order parameter as a function of temperature. Once established, future laser melting experiments will permit testing of the disorder trapping theory developed under this contract.

III. B2 and Related Phases in the Ti-Al-Nb System

Titanium aluminides (Ti_3Al and TiAl) with ~10 at% Nb additions have received considerable attention as potential low density, high strength and creep resistant materials. However, the phase equilibria in this ternary system is poorly understood. Because the presence of BCC-based phases in these alloys seems to play an important role in the deformation, in-depth studies of the BCC-based phase fields are being conducted. A series of alloys shown in Table 1 surrounding the composition Ti_2AlNb are being studied by TEM to determine the structure of phases present in arc cast, melt spun and heat treated samples.

Table 1 - Ti-Al-Nb Alloys Under Investigation

Ingot #	at% Ti	at% Al	at% Nb	ppm O	ppm N	ppm H
30	50 (51.1)	25 (23.9)	25 (25.0)	500	130	22
01	50 (50.6)	12.5 (12.2)	37.5 (37.2)	500	320	34
02	37.5 (38.1)	25 (24.3)	37.5 (37.6)	290	30	7
03	62.5 (63.5)	25 (24.2)	12.5 (12.3)	520	90	12
04	50 (51.4)	37.5 (36.2)	12.5 (12.4)	630	50	7

When complete, these results, combined with those from the University of Wisconsin by J. Perepezko and Y. A. Chang under DARPA sponsorship, will be combined with ternary phase diagram calculations performed under this contract to determine the ternary phase diagrams Ti-Nb-Al. Efforts during this contract period have been focused on the composition Ti_4Al_3Nb which is midway between TiAl and Ti_2AlNb (Alloy #04).

Detailed study of ω-type phases in Ti_4Al_3Nb

The study of phase equilibria in this system is complicated by the possibility of fast metastable ordering reactions of a chemical or a displacive type. Detailed studies have been conducted for Ti_3Al alloys with Nb substitutions of up to 20 at.% for Ti by Strychor et al.[1] and Banerjee et al.[2]. Both groups have reported the existence of a high temperature BCC or B2 phase; however, the details of the low temperature transformations were different due to differences in the heat treatment. More recent investigations indicate that the phase diagram of this Ti_3Al-Nb_3Al pseudobinary section is indeed quite complex [3-6].

In the present study we have investigated the decomposition of the high temperature B2 phase with composition Ti_4Al_3Nb during either cooling or low temperature annealing. This composition lies on the TiAl-TiNb pseudobinary section midway between the compositions TiAl and Ti_2AlNb. Alloys along this section were chosen because of previous work by Banerjee et al.[7] who showed that in B2 Ti-Al-Nb alloys, Ti tends to occupy one sublattice while Al and Nb tend to occupy the other sublattice. As already indicated in our previous preliminary report [8], the alloy exhibits some microstructural features similar to that found by Strychor and co-authors [1] for a Ti-25at%Al-12.5at%Nb alloy.

Strychor and coworkers found that when the cooling rate from the high temperature BCC phase is high enough, the transformation path developed during low temperature heat treatment can be completely different from that for slower cooling. At slower cooling rates the BCC phase first transforms martensitically to the HCP phase which subsequently orders to the DO_{19} phase. Partial decomposition of the DO_{19} phase to the orthorhombic (described first by Banerjee and co-authors [2]) is also possible. At higher cooling

rate (water quenching), the disordered BCC phase first orders to the B2 structure, and this seems to prevent the martensitic transformation to the hexagonal phase (however signs of a (110)<110> displacive instability corresponding to the hexagonal packing of atoms can be seen as 110 relrods and diffuse 1/2 110 reflections). Instead, the formation of an "ω-type" phase in the parent B2 matrix is observed.

If the "ω-type" phase forms by the well known mechanism of displacive ordering, i.e. by collapse of (111) plane pairs of the B2 phase, the result will be the ordered ω-phase (we will call it ω'), with a c-parameter twice that of the disordered ω phase. The structure of the ω' phase is shown in Fig. 1b, where its chemical ordering is assumed to be inherited from the B2 structure (Fig. 1a). The space group symmetry of the ω' phase would be P3m1 (#164), with 1a and 2d sites occupied with Ti and 1b and another 2d site occupied with 3/4 Al and 1/4 Nb. With this occupancy the space group remains the same even when the collapse of the (111) planes is complete (when the z parameter for the two d sites are 1/4 and 3/4). For disordered ω, the symmetry group changes to hexagonal when the collapse is complete.

For the trigonal P3m1 space group all reflections are allowed (including special positions) [9]. However, as was noted by Strychor and co-authors [1], the structure factor of the 1100 reflection for the ω' phase is zero because of the special occupancy of the sites inherited from the B2 phase. Observation of reflections at $1/3\langle 112\rangle_{BCC}$ positions in a selected area electron diffraction pattern (SADP) (corresponding to the 1100 reflection of the ω'-phase) led the authors [1] to suggest a secondary transformation of the ordered ω-phase to the $B8_2$ structure. This structure is shown in Fig. 1c and is closely related to the ordered ω'-phase but is based on an A_2B ordering. The space group for the $B8_2$ structure is hexagonal $P6_3/mmc$ (#194)

with reflection conditions such that the 1100 reflection is present, but odd 000ℓ reflections are absent. For the space group P3m1, odd 000ℓ reflections are present.

The purpose of this paper is to demonstrate that indeed the phase with the $B8_2$ structure is present in the Ti-Al-Nb system, probably as an equilibrium low temperature phase. However the mechanism of the low temperature decomposition of the B2 phase to the $B8_2$ is more complex than was suggested by Strychor et al [1]; viz., an intermediate trigonal phase, ω" occurs. This phase involves partial collapse of 111 planes and reordering from the B2. The structure of the ω" phase is shown in Fig. 1d, and was verified in the present research both by single crystal X-ray diffraction and by means of transmission electron microscopy.

(a) EXPERIMENTAL PROCEDURE - An alloy with the Ti_4Al_3Nb composition was prepared by arc melting. Approximately ten remelts were necessary to ensure mixing of the components. Pieces from the cast button were homogenized at 1400°C for three hours under 2/3 atm. gettered Ar gas. Precision of temperatures in that furnace is estimated to be about 20°C. It was found necessary to rest samples on a Y_2O_3 coated Al_2O_3 substrate to prevent reaction with Al_2O_3. Cooling was performed by lowering the samples out of the hot zone of the furnace into a lower chamber. The initial cooling rate was estimated to be about 400°C/min. Lower temperature heat treatments were performed on the homogenized (HT1) specimens. Two sets of specimens (HT2 and HT3) were treated at 1100°C. The former (HT2) were prepared in the same furnace as the HT1 specimens with a 1100°C treatment for 4.5 hours immediately after cooling from 1400°C followed by cooling to room temperature at ~400°C/min. The latter (HT3) were prepared by encapsulating Ta foil-

wrapped slices in evacuated and He-backfilled quartz tubes and heat treating at 1100°C for 4 days followed by a water quench. A fourth set of samples (HT4) were heat treated in tubes at 700°C for 26 days and water quenched. Sample HT1 had 630, 50 and 7 ppm of O,N and H respectively.

All four heat treated specimens (HT1-HT4) were studied by transmission electron microscopy (TEM). TEM thin foils were prepared by standard twin-jet electropolishing procedure using a 300 ml methanol, 175 ml n-butanol, 30 ml $HClO_4$ electrolyte at 0°C.

Optical and SEM/microprobe metallography of all four specimens was also performed because the scale of some of the microstructural details obtained at high temperatures was quite coarse.

The HT1 specimen has also studied using single crystal X-ray diffractometry[10]. For that purpose a small (<0.5 mm) cube was cut out of a single grain as observed by optical microscopy.

(b) RESULTS - Microstructures of samples annealed at 1400 and 1100°C - All specimens cooled from high temperature (HT1, HT2 and HT3) go through a phase transformation during cooling. This is evident from the presence of two different microstructural scales - one on the order of 10^3 to 10^2 μm observed by optical metallography, and another on the order of 10^{-1} μm or less, observed by TEM.

The coarse scale represents the microstructure present at high temperature and consists of large single phase grains for the 1400°C sample (HT1), or large grains of the same phase (as will be evident later) with an included second constituent comprising about 6% of the sample volume for the 1100°C samples (HT2 and HT3). The second constituent occurred in two morphologies: particles of DO19 phase or a mixture of DO19 and $L1_0$ phases

based on the Ti-Al system. The two phase structures were not identified as such until the TEM work was done.

The fine scale microstructure observed by TEM is a result of the decomposition of the B2 matrix during cooling from temperature. As recent investigations have shown [8], the B2 phase exists as an equilibrium high temperature phase over a large compositional field of the Ti-Al-Nb system. For several alloy compositions the B2 phase was either found directly in quenched specimens, or its existence was inferred from its decomposition product. The later is the case for the presently investigated composition. Selected area diffraction (SAD) with a large aperture shows patterns with strong reflections corresponding to the B2 lattice and additional weaker superlattice reflections; e.g., $\langle 110 \rangle_c$ and $\langle 111 \rangle_c$ cubic zone axes shown in Fig. 2a-d. According to Strychor et al.[1] who showed similar diffraction for another Ti-Al-Nb alloy, the superlattice reflections can be described as belonging to the ordered omega-type phase with the following parameters for its hexagonal lattice: a=0.46 nm and c=0.58 nm (the c-parameter is twice that of disordered omega-phase).

The omega-type phase occurs in the usual orientation relationship with the parent cubic phase: $\langle 111 \rangle_c || (110)_h$ and $(110)_c || (1120)_h$, which produces four rotational variants. The SAD patterns are superpositions of these four variants of the omega-type phase. The pattern, $\langle 110 \rangle_c$ (Fig.2a), consists of two <1120> and two <1102> zone axes, and the pattern, $\langle 111 \rangle_c$ (Fig.2b), consists of one <0001> and three <2201> zone axes. The <1102> and <2201> patterns of the omega-type phase are practically indistinguishable from the <110> and <111> patterns of the B2 phase as seen in zero order Laue zones (but can be distinguished by a difference in the radius of higher order Laue zones). Some reflections in the patterns can be the result of double or

dynamic diffraction; e.g., in the $<110>_c$ pattern, the $1/3<hh0>_c$ and $1/3<100>_c$ reflections are caused by double diffraction, as verified by their disappearance after tilting along this row of reflections.

TEM observation shows that the microstructures of the HT1 and the matrix of the HT2 specimens are similar in spite of different heat treatments and slight differences in composition due to the formation of the DO_{19} and $L1_0$ phases in HT2. (Ti-36.5at%Al-12.5at%Nb for the matrix phase of the HT2 specimen compared to Ti-36.2at%Al-12.4at%Nb for HT1 as measured by microprobe using elemental standards). Their microstructures consist of small (~0.2 μm) domains producing complex contrast in a bright-field image, Fig.3a, due to overlapping through the TEM foil thickness. The domains can be clearly seen using dark-field imaging with a reflection belonging only to one rotational variant of the omega-type phase, e.g., with the 1100 reflection. Such dark-field images are shown in Fig.3b where some but not all imaged regions contain boundaries. Because only one rotational variant is imaged, these boundaries separate translational subvariants of the same rotational variant. Two type of interfaces can be recognized: those having relatively straight boundaries and forming triple junctions (A), and those usually having large curvature (B). The presence of triple junctions implies the existence of at least three translational domain subvariants for each rotational domain (as imaged in dark field in Fig. 3b). This observation is inconsistent with the $B8_2$ phase which only has two translational domain subvariants.

As was discussed above, it is important to find out if the reflections 0001 are forbidden in order to determine the structure of the omega-type phase. For that purpose tilting along a row of 0001 (or 111_c) reflections was performed in order to eliminate roots for double diffraction. As can be seen in Fig. 4a where only the one row is exited, no extinction of odd reflections

is observed. However the result can be due to the double diffraction between two variants, viz., 0002 of one variant and 0221 (= 111_c) of the other variant. To eliminate this possible effect, microdiffraction from a thin area was used in order to obtain diffraction from only a single domain. The result is shown in Fig.4b, where odd 000ℓ reflections are clearly seen for one variant, and only the 0003 (actually 0221) reflection for another variant, Fig.4c. The presence of these reflections also suggest that the phase has trigonal symmetry.

From dark-field imaging of a single rotational variant, it is evident that the omega-type phase is the major phase occupying most of matrix. However from the TEM observation it is difficult to decide if there is a retained B2 or BCC phase mixed with the ω-type phase. A cubic phase can not be imaged separately because of perfect overlapping of its reflections with those of the omega-type phase. Morphologically there is no evidence for the presence of a retained B2 phase. It is in principle possible to detect the cubic phase using convergent beam diffraction and analysis of HOLZ reflections. This will not give an overall morphological picture and the interpretation will be complicated by possible overlapping of domains. As will follow however, results from single crystal X-ray diffraction suggest that a certain amount of the cubic phase was retained in the HT1 sample.

The high cooling rate of the water quenched HT3 specimen was not sufficient to prevent decomposition of the high temperature cubic phase to the omega-type phase. This is evident from the SAD patterns shown in Fig.2c,d. The patterns can be compared with those in Fig.2a,b from the HT1 specimen since they are of the same cubic orientation. The HT3 quenched specimen has the same type of omega-type reflections, however they are rather diffuse maxima rather than sharp spots. For the $[110]_c$ zone axis no

double diffraction spots like $1/3\langle 110\rangle_c$ or $1/3\langle 100\rangle_c$ are present, but there is additional diffuse intensity in the form of spot streaking, arcs and diffuse maxima like in $1/2\langle 110\rangle_c$ and $1/2\langle 112\rangle_c$ in Fig.2c. Comparison of the $[111]_c$ zone axis patterns shows that the 1100 reflections are much weaker for the HT3 specimen than for the HT1 or HT2 specimens. Dark-field images using a strong reflection (belonging simultaneously to several variants and possibly to the cubic phase) in a two beam condition have contrast consisting of striations, as shown in Fig.5a. Dark-field images using a reflection belonging only to one variant of the omega-type phase show a uniform distribution of very small diffuse particles (~2-3 nm), Fig.5b. Thus although the quenched samples contain an ω-type phase, its morphology and diffraction are different from more slowly cooled samples.

Single crystal X-ray diffraction study of the structure of the omega-type phase in the HT1 specimen - Single crystal x-ray diffraction was performed on a sample (HT1) cooled from 1400°C using Mo K_α radiation. The structural refinement was performed[10] using the full-matrix least-squares program contained in the TEXRAY system of programs. The final R value was 0.032. The results are summarized in Table 2.

Table 2 - Summary of Single Crystal Diffraction Results

1. P3m1 space group, a=0.4553 nm, c=0.5534 nm

2. Occupancy based on assumptions of (a) a composition of Ti_4Al_3Nb, (b) only two species on each site and (c) equal representation of all twins/variant:

1a	0.88Ti + 0.12Nb	0	0	0
1b	0.68Nb + 0.32Al	0	0	1/2
2d	0.97Al + 0.03Nb	1/3	2/3	0.2245
2d	Ti	1/3	2/3	0.7175

3.Residual B2 or BCC phase

With the exception of whether residual B2 or BCC exists, the TEM and X-ray results are consistent and show that the matrix phase of alloys cooled from 1400 or 1100°C, designated ω'', is a partially collapsed trigonal ω phase with an atomic arrangement different than, but related to, the precursor B2 phase.

Microstructure of samples annealed at 700°C - The microstructure of sample HT4 as observed by optical microscopy is shown in Fig 6. Large grains (not shown) with a size established during the 1400°C treatment are still present. Within these grains are an irregular network and a precipitate structure too fine for optical microscopy. The network boundaries appear diffuse in the optical micrographs, and in fact seem to consist of layers different from the precipitate structure.

TEM observation of the matrix phase shows that the microstructure has features similar to those of the HT1 and HT2 specimens, i.e. predominantly a multidomain structure of an omega-type phase, Fig.7a,b. The omega-type phase has lattice parameters and orientation relationships practically identical to those in the HT1 and HT2 specimens. However the domains have a size that is almost an order of magnitude coarser than in the HT1 and HT2 specimens (~0.6 μm in size). As will be shown below, the size of these domains results from a phase transformation process from the ω'' phase. The domains are large enough to perform safe convergent beam symmetry analysis from a thick single crystal (no interference from interfaces other than the TEM foil surface). Fig.8 shows large and small magnification convergent beam electron diffraction (CBED) patterns for the [0001] and [1120] zone axis orientations. As is clearly seen from the patterns, the whole pattern

symmetry is 6mm for the [0001] orientation and 2mm for the [1120] orientation. These results are inconsistent with the trigonal omega-type phase determined for the HT1 sample by x-ray analysis. (For the trigonal space group P3m1, the CBED whole pattern symmetry must be 3m and 2). The observed whole pattern symmetries establish unambiguously that the phase has hexagonal point group symmetry 6/mmm.

Additional confirmation that the matrix phase in the 700°C sample has hexagonal symmetry is the absence of odd 000ℓ reflections (Fig.9) under diffraction conditions similar to those shown in Fig.4b, suggesting that they are kinematically forbidden. Moreover, the observation of dynamic extinction in a kinematically forbidden 0001 reflection in the form of a black cross (Fig.8c) for the [1120] zone axis, which is a result of the simultaneous presence of a screw axis and a glide plane in the structure, can be explained only by the space group $P6_3/mmc$ [9]. The $P6_3/mmc$ space group is that of the $B8_2$ structure proposed by Strychor and co-authors for the Ti-Al-Nb omega-type phase [1], and is shown in Fig.1c.

In addition to the transformation of the omega-type phase from trigonal to hexagonal symmetry, there are two other morphologically distinct constituents that formed during annealing at 700°C. One appears in the form of needles growing in a common orientation within the hexagonal matrix, Fig.10a. The phase was identified by microdiffraction, Fig.10b, as a $L1_0$ phase probably based on TiAl. The other constituent has a peculiar band morphology shown in Fig.11a. It probably forms the network seen in the optical micrographs, Fig.6. Higher magnification shows that the bands are composed of alternating layers of crystals of either different orientation or crystal structure, Fig.11b. Some crystals protrude from the band into the surrounding matrix. Fig.11c shows a SAD pattern taken from the area shown in

Fig.11b. With the help of microdiffraction the pattern was identified as the superposition of three different diffraction patterns: the [2201] zone axis of the $B8_2$ matrix phase (M), the [1120] zone axis of the DO19 Ti_3Al band phase (B), and the [011] zone axis of the TiAl $L1_0$ phase with two (111) twin variants (L). The orientation relationship is such that the (0001) plane of the DO19 phase is parallel to the (111) of the $L1_0$ phase and to the (1120) (or (1012)) of the $B8_2$ phase. The parallel interfaces inside the band are basai planes of the hexagonal DO19 phase, and probably are stacking faults and boundaries between the DO19 and $L1_0$ phases. The presence of the twin variants of the $L1_0$ phase suggests that the band was formed either by simultaneous growth of two coherent phases, DO19 and $L1_0$, or by the formation of the DO19 phase and subsequent coherent precipitation of the $L1_0$ phase or the reverse. The second mechanism produces a well-known microstructural feature in Ti-Al alloys [11].

The first stages of this transformation to the described three phase microstructure were observed in some places in the HT2 specimens, which were probably subjected to slower cooling than in the regions whose microstructure was described under the 1100°C treatment. Fig.12a shows a dark-field image in a condition where only one rotational variant of the omega-type phase is imaged. Some domains are noticeably larger, suggesting a discontinuous coarsening process. However careful CBED analysis shows that the large domains have the hexagonal symmetry of the $B8_2$ phase while the small domains have trigonal symmetry. Note that the new phase has a structure of translation domain boundaries different from that observed for the trigonal phase, Fig.3. There are no triple junctions of the boundaries, consistent with the fact that within in one rotational domain variant (as imaged in dark field), there are only two tranlational domain variants for the $B8_2$

structure. The new phase usually forms along some heterogeneity, as shown in Fig.12b. In some places the heterogeneity is another precipitated phase, as shown in Fig.12c. The phase was identified by SAD and microdiffraction as the $L1_0$ phase, similar to that found in the annealed HT4 specimen.

(c) INDENTATION TESTING - High load (120 Kg) diamond pyramid indentation testing provides a useful method for screening the toughness of alloys (B. R. Lawn and D. B. Marshall, J. Amer. Cer. Soc. 62 (1979), 347). Fig 13 shows the indentations for the five alloys listed in Table 1 which have been heat treated for 4 days at 1100°C. The Vickers hardness is shown and NC indicates that no cracks where generated. In the sample of composition Ti-37.5Al-12.5Nb the cracks extended across the sample indicating a K_c close to zero. According to the above section this sample is primarily an ω-type phase. In the sample of composition Ti-25Al-37.5 the cracks had finite length permitting an estimate for K_c of 5 MPa$\sqrt{m}$. According to research reported previously, this sample consists of a BCC or B2 matrix with σ-Nb_2Al phase. Figure 14 shows that all samples of composition Ti_2AlNb failed to crack under 120 Kg indentation. One notes the high hardness and refined slip seen in the sample treated at 800°C compared to the sample treated at 1400°C.

(d) FUTURE RESEARCH - Future work will involve an analysis of the phases present at 700°C after a one month annealing for the Ti_2AlNb composition. Here an orthorhombic phase forms a complex two-phase microstructure with the DO_{19} α_2 phase. The calculated ternary phase diagram Ti-Al-Nb which was presented in a previous report will be modified to be consistent with this new data and other data generated by J. H. Perepezko and Y. A. Chang at the University of Wisconsin, Madison, under DARPA sponsorship.

IV. Phase Diagram Modeling

As part of an overall objective to produce calculations of the Ti-Al-Nb and Nb-Al-Si ternary systems which are consistent with experimental data, the Nb-Al and Nb-Si binary systems have been reevaluated and modeled thermodynamically. This information should provide a sound basis for the optimization of processing and microstructure in these systems.

(a) The Nb-Al (Niobium - Aluminum) System

The Nb-Al System is a relatively simple system with six phases:

- The liquid L
- The bcc (Nb) solid solution, which dissolves up to ~21.5 at.% Al at 2060 °C
- The Nb_3Al phase, with the cubic Cr_3Si structure and a maximum range of homogeneity from 18.6 at.% Al below 1500 °C to 25 at.% Al at 1940 °C, it forms peritectically from the melt and (Nb) at 2060 °C
- The Nb_2Al phase, with the tetragonal σ-CrFe structure and a maximum range of homogeneity from 30 at.% Al below 1500 °C to 42 at.% Al at 1590 °C, it forms peritectically from the melt and Nb_3Al at 1940 °C
- The $NbAl_3$ phase, with the tetragonal $TiAl_3$ structure and a narrow range of homogeneity with a width of ~1 at.%, it forms congruently from the melt at 1680 °C
- The fcc (Al) solid solution with extremely limited solubility of Nb

The assessed phase diagram (Figs 15 - 19) is based on a review of the literature [66Lun, 68Sve, 76Yer, 80Jor, 88Mur]. Although the existence of the three intermediate compounds and the solid-solid phase boundaries of (Nb), Nb_3Al and Nb_2Al are quite well established, the liquidus and reaction temperatures have not been precisely established. Such uncertainties are indicated by dotted lines in the assessed phase diagram.

In splat quenched samples supersaturated solutions of (Nb) (up to 27 at.% Al) and Nb_3Al (27.5 at.% Al) were observed [88Sch]. Supersaturation of the Nb_3Al phase was also obtained using sputter deposited Nb/Al multilayer samples [86Bor, 88Yoo], however there is disagreement whether with this method a supersaturated (Nb) can be obtained.

The Nb_3Al phase is a superconducting compound with a transition temperature of 18.6 K.

Invariant Points of the Assessed Nb-Al Phase Diagram

Reaction	Compositions at.% Al			Temperature °C	Reaction type
(Nb) + L → Nb_3Al	21.5	28	22.5	2060±10	Peritectic
Nb_3Al + L → Nb_2Al	25	32	32	1940±10	Peritectic
L → Nb_2Al + $NbAl_3$	54	42	75	1590±5	Eutectic
L + $NbAl_3$ → (Al)	(99.96)	75	(99.94)	661.4±0.5	Peritectic
L → $NbAl_3$		75		1680±5	Congruent point
L → (Nb)		0		2469	Melting point
L → (Al)		100		660.452	Melting point

Note: Data that are tentative are enclosed in parenthesis

Nb-Al Crystal Structure Data

Phase	Composition at.% Al	Pearson symbol	Space group	Struktur-bericht designation	Proto type
(Nb)	0 - 21.5	cI2	Im-3m	A2	W
Nb_3Al	18.6 - 25	cP8	Pm-3n	A15	Cr_3Si
Nb_2Al	30 - 42	tP30	$P4_2/mnm$	...	σ-CrFe
$NbAl_3$	75	tI8	I4/mmm	DO_{22}	$TiAl_3$
(Al)	100	cF4	Fm-3m	A1	Al

Thermodynamic Modeling of the Nb-Al System

For the calculation of the Nb-Al system the liquid, the bcc (Nb) and fcc (Al) phase were described using regular solution type models. Three polynomial terms for the enthalpy and two for the entropy were used for the liquid, two polynomial terms for the enthalpy and one for the entropy were used for the bcc (Nb) phase and only one term for the enthalpy of fcc (Al) was used. The two intermetallic compound Nb_3Al and Nb_2Al reveal relatively wide ranges of homogeneity and were therefore modeled with the Wagner-Schottky model. Nb_3Al was described with two sublattices, allowing substitutional solution to occur on each of these sublattices. Nb_2Al was described with three sublattices of the stoichiometry $Nb_{16}Al_{10}Nb_4$, where substitutional solution was allowed on the first two sublattices. For each of these two intermetallic compounds six parameters were used: enthalpy and entropy of formation of the compound without any substitution occurring and enthalpy and entropy of formation for the substitutional atoms. $NbAl_3$ was assumed to be stoichiometric.

For the optimization of the Nb-Al system the phase diagram data of [59Gla, 61Bar, 66Lun, 70Mul, 71Wik] were not used, since they are contradictory to the data of [68Sve, 76Yer, 80Jor, 88Mur], which are in relative good agreement. The partial Gibbs energy data of [74Mal, 78Nik] were also not used for the optimization because they are in disagreement with the data of [82Shi] who measured also the temperature dependence in a wide composition range, for compositions > 34 at.% Al, these data were omitted in the optimization, since it is doubtful that these data represent equilibrium. The enthalpies of mixing of the liquid phase reported by [85Sud] were omitted during the optimization, since the showed inconsistency with the phase diagram and the other thermodynamic data.

The Nb-Al system was optimized at the beginning by a least squares method, then the parameters of the Nb_3Al and Nb_2Al phases were refined using trial and error. With the as derived analytical description the phase diagram and the thermodynamic functions were calculated, except for the temperature of the eutectic $L \rightarrow Nb_2Al + NbAl_3$ the phase diagram and the thermodynamic quantities can be reproduced within the experimental error.

Analytical Description of the Nb-Al System

General formula for the Gibbs energy: $G = \sum_i X(x,n)_i * (H_i - S_i * T)$

with: $\sum_i n_j^i = x_j$

The reference state for all phases is bcc Nb and liquid Si.

The lattice stabilities for the pure elements are from Saunders et al. [88Sau].

Coefficients adjusted in the optimization are underlined.

Liquid, Substitutional Solution (Nb,Al)

$X(x,n)_i$	H_i	S_i
x_{Nb}	30000.00	10.90900
x_{Al}	0.00	0.00000
$\sum_j x_j * \ln(x_j)$	0.00	-8.31451
$x_{Nb}x_{Al}$	<u>-133412.60</u>	<u>-32.63330</u>
$x_{Nb}x_{Al}*(x_{Nb}-x_{Al})$	<u>6327.70</u>	<u>8.28036</u>
$x_{Nb}x_{Al}*(x_{Nb}-x_{Al})^2$	<u>27496.90</u>	0.00000

bcc (Nb), Substitutional Solution (Nb,Al)

$X(x,n)_i$	H_i	S_i
x_{Nb}	0.00	0.00000
x_{Al}	-628.00	-6.66300
$\sum_j x_j * \ln(x_j)$	0.00	-8.31451
$x_{Nb}x_{Al}$	<u>-179533.30</u>	<u>-47.30541</u>
$x_{Nb}x_{Al}*(x_{Nb}-x_{Al})$	<u>25485.20</u>	0.00000

fcc (Al), Substitutional Solution (Nb,Al)

$X(x,n)_i$	H_i	S_i
x_{Nb}	22000.00	2.20000
x_{Al}	-10711.00	-11.47300
$\sum_j x_j * \ln(x_j)$	0.00	-8.31451
$x_{Nb}x_{Al}$	<u>-80000.00</u>	0.00000

Nb_3Al, Wagner-Schottky Compound $(Nb,Al)_3(Al,Nb)_1$

$X(x,n)_i$	H_i	S_i
$\sum_l \sum_j n_j^l * \ln(n_j^l)$	0.00	-8.31451
1	-37335.20	-8.77215
n_{Nb}^2	149341.00	28.34497
n_{Al}^1	53098.20	11.50000

Nb_2Al, Wagner-Schottky Compound $(Nb,Al)_{16}(Al,Nb)_{10}(Nb)_4$

$X(x,n)_i$	H_i	S_i
$\sum_l \sum_j n_j^l * \ln(n_j^l)$	0.00	-8.31451
1	-49113.10	-12.51828
n_{Nb}^2	141000.00	23.30000
n_{Al}^1	52946.80	4.00000

$NbAl_3$, Stoichiometric Compound Nb_1Al_3

$X(x,n)_i$	H_i	S_i
1	-48626.20	-15.31191

(b) The Nb-Si (Niobium - Silicon) System

The Nb-Si system consists of seven phases:

- The liquid L
- The bcc (Nb) solid solution which dissolves only few Si (up to 1.2 at.% Si at 1920 °C
- The Nb_3Si phase with the tetragonal Ti_3P structure. It forms peritectically from the melt and βNb_5Si_3 at 1940 °C and decomposes eutectoidally into (Nb) and αNb_5Si_3 at 1770 °C
- The αNb_5Si_3 phase with the tetragonal Cr_5B_3 structure and forms peritectoidally from Nb_3Si and βNb_5Si_3 at 1980 °C. Its narrow range of homogeneity extends from 37.5 to 39.5 at.% Si at 1650 °C
- The βNb_5Si_3 phase with the tetragonal W_5Si_3 structure. It forms congruently from the melt at 2520 °C and decomposes eutectoidally into αNb_5Si_3 and $NbSi_2$ at 1650 °C. Its maximum range of homogeneity extends from 37.5 to 40.5 at.% Si at 1900 °C
- The $NbSi_2$ phase with the hexagonal $CrSi_2$ structure. It forms congruently from the melt at 1940 °C
- The dia (Si) with the cubic diamond structure and nil solubility for Nb

The liquidus of the Nb-Si system was determined in two experimental studies, [55Kna] measured pyrometrically the temperature of melting and the accuracy of the temperatures reported is estimated to be greater than ±50 °C. [80Koc] used high temperature DTA and give an accuracy of ±20 °C, these data were used for the evaluated phase diagram (Fig.20).

Invariant Points of the Assessed Nb-Si Phase Diagram

Reaction	Compositions at.% Si			Temperature °C	Reaction type
$L \rightarrow (Nb) + Nb_3Si$	17.5	1.2	25	1920±20	Eutectic
$L + \beta Nb_5Si_3 \rightarrow Nb_3Si$	~19	~37.5	25	1980±20	Peritectic
$Nb_3Si + \beta Nb_5Si_3 \rightarrow \alpha Nb_5Si_3$	25	~37.5	~37.5	1940±20	Peritectoid
$Nb_3Si \rightarrow (Nb) + \alpha Nb_5Si_3$	25	0.5	37.5	1770±20	Eutectoid
$L \rightarrow \beta Nb_5Si_3 + NbSi_2$	57	40.5	66.7	1900±20	Eutectic
$\beta Nb_5Si_3 \rightarrow \alpha Nb_5Si_3 + NbSi_2$	39.5	~40	66.7	1650±15	Eutectoid
$L \rightarrow NbSi_2 + (Si)$	98	66.7	100	1400±10	Eutectic
$L \rightarrow \beta Nb_5Si_3$		~37.5		2520±25	Congruent poi
$L \rightarrow NbSi_2$		66.7		1940±20	Congruent poi
$L \rightarrow (Nb)$		0		2469	Melting point
$L \rightarrow (Si)$		100		1414	Melting point

Nb-Si Crystal Structure Data

Phase	Composition at.% Si	Pearson symbol	Space group	Struktur-bericht designation	Proto type
(Nb)	0 - 1.2	cI2	Im-3m	A2	W
Nb_3Si	25	tP32	$P4_2/n$	...	Ti_3P
αNb_5Si_3	~37.5 - 39.5	tI32	I4/mcm	$D8_l$	Cr_5B_3
βNb_5Si_3	~37.5 - 40.5	tI32	I4/mcm	$D8_m$	W_5Si_3
$NbSi_2$	66.7	hP9	$P6_222$	C40	$CrSi_2$
(Si)	100	cF8	Fd-3m	A4	C

Thermodynamic Modeling of the Nb-Si System

For the calculation of the Nb-Si System the liquid was described using the quasi-subregular model and all the solid phases were assumed to be stoichiometric, since they all reveal no or only very small ranges of homogeneity.

The phase diagram data of [80Koc] and the enthalpies of formation of [72Gor] were used for the least squares optimization of the Nb-Si system. The calculated and the experimental phase diagram agree very well, while the calculated enthalpies of formation of aNb_5Si_3 and $NbSi_2$ differ more the experimental error reported by [72Gor]

Calculated and Measured Enthalpies of Formation at 25 °C

Phase	$\Delta H_{meas.}$ J/mol of atoms	$\Delta H_{calc.}$ J/ mol of atoms
αNb_5Si_3	-63858±11700	-43137
$NbSi_2$	-52000±15000*	-59933

* Enthalpy derived from the value reported for the two-phase equilibrium $\alpha Nb_5Si_3 + NbSi_2$

Analytical Description of the Nb-Si System

General formula for the Gibbs energy: $G = \sum_i X(x,n)_i * (H_i - S_i * T)$

The reference state for all phases is bcc Nb and liquid Si.

The lattice stabilities for the pure elements are from Saunders et al. [88Sau].

Coefficients adjusted in the optimization are underlined.

Liquid, Substitutional Solution (Nb,Si)

$X(x,n)_i$	H_i	S_i
x_{Nb}	30000.00	10.90900
x_{Si}	0.00	0.00000
$\sum_j x_j * \ln(x_j)$	0.00	-8.31451
$x_{Nb}x_{Si}$	<u>-197387.10</u>	<u>-42.33861</u>
$x_{Nb}x_{Si}*(x_{Nb}-x_{Si})$	<u>-116757.40</u>	<u>-58.17759</u>

(Nb), Stoichiometric Compound Nb_1Si_0

$X(x,n)_i$	H_i	S_i
1	0.00	0.00000

(Si), Stoichiometric Compound Nb_0Si_1

$X(x,n)_i$	H_i	S_i
1	-50208.00	-29.76200

Nb_3Si, Stoichiometric Compound Nb_3Si_1

$X(x,n)_i$	H_i	S_i
1	<u>-36991.30</u>	<u>-5.45877</u>

αNb_5Si_3, Stoichiometric Compound Nb_5Si_3

$X(x,n)_i$	H_i	S_i
1	<u>-61964.80</u>	<u>-11.35889</u>

βNb_5Si_3, Stoichiometric Compound $Nb_{31}Si_{19}$

$X(x,n)_i$	H_i	S_i
1	<u>-58966.70</u>	<u>-9.78875</u>

$NbSi_2$, Stoichiometric Compound Nb_1Si_2

$X(x,n)_i$	H_i	S_i
1	-93405.20	-27.02926

REFERENCES

1. R. Strychor, J.C. Williams and W.A. Soffa, Met. Trans. 19A (1988) 225.

2. D.Banerjee, A.K. Gogia, T.K. Nandi and Joshi, Acta Met. 36 (1988) 871.

3. M.J. Kaufman, T.F.Broderick, C.H.Ward, R.G. Rowe and F.H. Froes, Sixth World Conference on Titanium, Cannes.

4. M.J. Kaufman, AFWAL Technical Report-88-4113, (1988).

5. D. Banerjee, T.K. Nandy, A.K. Gogia and K. Muraleedran, Met. Trans. in press.

6. M.J.Kaufman et al., Mat. Res. Soc. Proc..in press.

7. Banerjee, T.K. Nandy and A.K. Gogia, Scripta Met. 21 (1987) 597.

8. L.A. Bendersky and W.J. Boettinger, Mat. Res. Soc. Proc., in press.

9. International Tables of Crystallography

10. C. B. Shoemaker, to be published.

11. M.J. Blackburn, in R.J. Jaffee and N.E. Promisel (eds.), The Science, Technology and Application of Titanium, Pergamon, Edinburgy, 1970, p. 633.

59Gla V.M. Glazov, V.N. Vigdorovich and G.A. Korol'kov, Russ. J. Inorg. Chem. 4 (1959) 730-732

61Bar V.V. Baron and E.M. Saviskii, Russ. J. Inorg. Chem. 6 (1961) 90-92

66Lun C.E. Lundin and A.S. Yamamoto, Trans. AIME 236 (1966) 863-872

68Sve V.N. Svechnikov, V.M. Pan and V.I. Latiesheva, Metallofiz. 2 (1968) 54-61

70Mul A. Mueller, Z. Naturforsch. 25a (1970) 1659-1669

71Wik A. Wicker, C. Allibert and J.Driole, C. R. Acad. Sc. Paris 272 (1971) 1711-1713

72Gor O.S. Gorelkin, A.S. Dubrovin, O.D. Kolesnokova, Yu.Ya. Demidov and N.A. Chirkov, Proizvodstvo Ferrosplavov (Celjabinsk) (1972) 123-137

74Mal G.A. Malets, Vesti. Akad. Nauk B.SSR, Ser. Khim Nauk (1974) No.6, 127-129

75Gel G.A. Gelashvili and Zh.I. Dzneladze, Soviet Powder Metall. Crem. 14 (1975) 732-737

76Kok L. Kokot, R. Horyn and N. Iliew, J. Less-Common Met. 44 (2976) 215-219

76Yer V.N. Yremenko, Ya.V. Natanzon and V.I. Dybkov, J. Less-Common Met. 50 (1976) 29-48

78Nik G.I. Nikolaev and N.V. Bodrov, Russ. J. Phys. Chem. 52 (1978) 821-823

80Jor J.L. Jorda, R. Fluekiger and J. Muller, J. Less-Common Met. 75 (1980) 227-239

82Shi I. Shilo, H.F. Franzen and R.A. Schiffman, J. Electrochem. Soc. 129 1608-1613

85Sud V.S. Sudavstova, G.I. Batalin and V.S. Tutevich, Russ. Metall. (1985) No.5, 183-185

86Bor R. Bormann, H.U. Krebs and A.D. Kent, Adv. Cryog. Eng. 32 (1986) 1041-1047

88Mur J.L. Murray, private communication of data from L.A. Willey, 1988

88Sau N. Saunders A.P. Miodownik and A.T. Dinsdale, CALPHAD 12 (1988) 351-374

88Sch K. Schulze, G. Mueller and G. Petzow, Z. Metallkde 79 (1988) 763-766

88Yoo I.M. Yoonsoon, P.E. Johnson, L.T. McKnelly, Jr. and J.W. Morris, Jr., J. Less-Common Met. 139 (1988) 87-95

55Kna A.G. Knapton, Nature 175 (1955) 730-730

72Gor O.S. Gorelkin, A.S. Dubrovin, O.D. Kolesnokova, Yu.Ya. Demidov and N.A. Chirkov, Proizvodstvo Ferrosplavov (Celjabinsk) (1972) 123-137

80Koc Yu.A. Kocherzhinskiy, L.M. Yupko and E.A. Shishkin, Russ. Metall. (1980) No.1, 184-188

88Sau N. Saunders A.P. Miodownik and A.T. Dinsdale, CALPHAD 12 (1988) 351-374

FIGURE CAPTIONS

Fig. 1. Projections of (a) B2, (b) hypothetical ω', (c) $B8_2$ (d) ω'' crystal structures in the $<110>_c$ or $<1120>_h$ direction. Different size circles represent different site occupancies.

Fig. 2. SADP's from decomposed B2 phase of composition Ti_4Al_3Nb. (a,b) cooled from 1400°C at ~400°C/min. (c,d) water-quenched from 1100°C.

Fig. 3. Microstructure of alloy cooled from 1400°C. TEM. (a) Bright-field, (b) dark-field of one rotational variant.

Fig. 4. Single row excitation showing presence of odd (000ℓ) reflections.

Fig. 5. Microstructure of alloy quenched from 1100°C showing striations and discrete ω-type particles. TEM. SADP's are shown in Fig. 2c and 2d.

Fig. 6. Optical micrograph of alloy annealed at 700°C.

Fig. 7. (a) TEM micrograph of the matrix phase of an alloy annealed at 700°C showing multi-domain structure. (b) SADP.

Fig. 8. High (a,c) and low (b,d) magnification CBED patterns in [0001] and [1120] orientations from a single domain of the matrix phase in an alloy annealed at 700°C. The patterns are consistent with point group symmetry 6/mmm.

Fig. 9. Single row excitation showing absence of odd (000ℓ) reflections.

Fig. 10. (a) Needles observed in alloy annealed at 700°C and (b) identified as the $L1_0$ phase.

Fig. 11. (a,b) Unusual network structure observed in alloy annealed at 700°C. (c) SADP showing superposition of $B8_2$, $L1_0$ and DO_{19} phases.

Fig. 12. (a) Large $B8_2$ domains adjacent to fine ω'' domains. (b) Formation of $B8_2$ domains along an unidentified heterogeneity and (c) along a plate of the $L1_0$ phase.

Fig. 13. 120 Kg hardness impressions in Ti-Al-Nb Alloys of the indicated compositions which were heat treated at 1100°C for 4 days.

Fig. 14. 120 Kg hardness impressions in Ti_2AlNb with the indicated heat treatments. The samples did not crack and the scale of slip has been refined by the low temperature heat treatment.

Fig.15. Calculated and measured phase diagram of the Nb-Al system.

Fig.16. Calculated and measured Al-rich part of the Nb-Al phase diagram.

Fig.17. Calculated and measured enthalpies of formation of the solid phases at 25 °C.

Fig.18. Calculated and measured partial Gibbs energies of Al in the solid phases at 1727 °C (2000 K).

Fig.19 Calculated and measured partial Gibbs energies of Al in the two-phase equilibria of the solid phases.

Fig.20 Calculated and measured phase diagram of the Nb-Si system.

V. Fiscal Status

(1) Amount currently provided for contract program

$150,000 for period February 9, 1987 to September 30, 1987.

$200,000 for period October 1, 1987 to September 30, 1988.

$200,000 for period October 1, 1988 to September 30, 1989

(b) Expenditure and commitment during October 1, 1988 to March 31,1989

$100,000

(c) Estimated funds required to complete this work

April to June 1989	$50,000
July to September 1989	$50,000
October to December 1989	$50,000

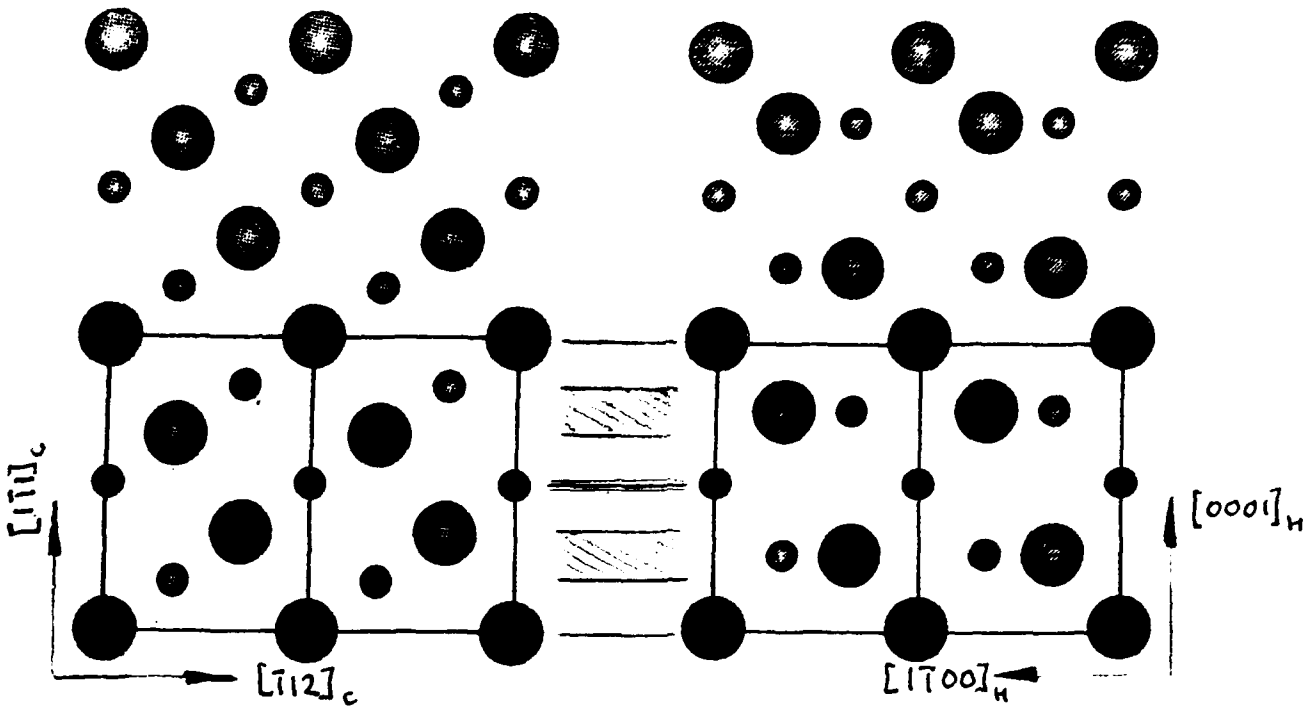

B2, $Pm\bar{3}m$

omega', $P\bar{3}m1$ (any z)
$F(0001)\neq 0$, $F(1\bar{1}00)=0$

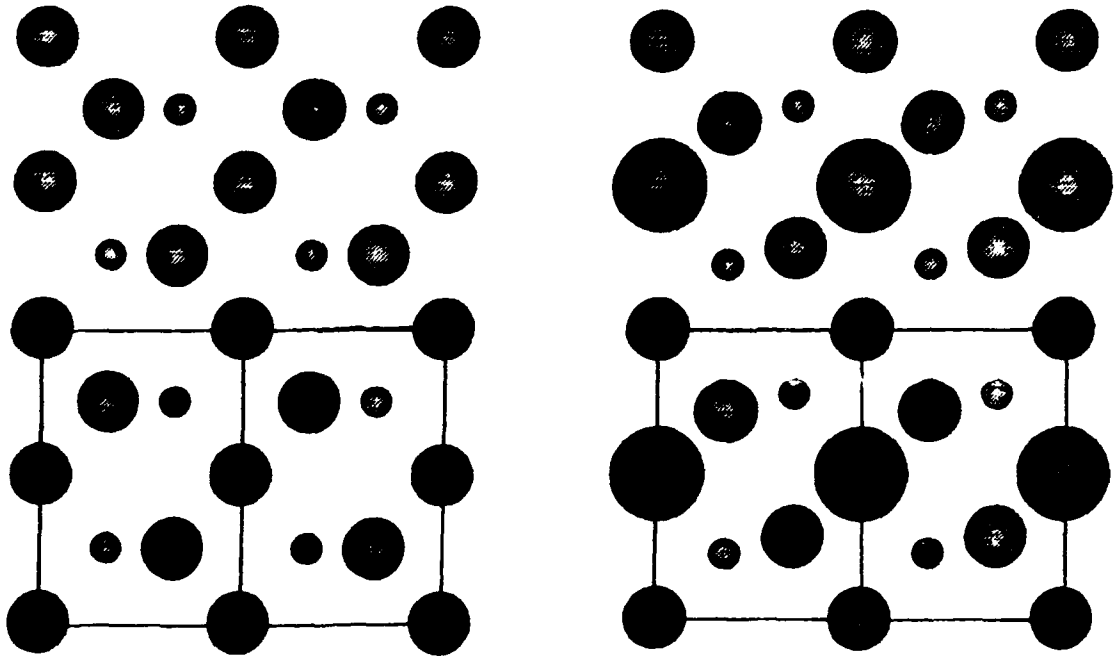

$B8_2$, $P6_3/mmc$
$F(0001)=0$, $F(1\bar{1}00)\neq 0$

omega'', P3m1
$F(0001)\neq 0$, $F(1\bar{1}00)\neq 0$

Fig. 1. Projections of (a) B2, (b) hypothetical ω', (c) $B8_2$ (d) ω'' crystal structures in the $<110>_c$ or $<1120>_h$ direction. Different size circles represent different site occupancies.

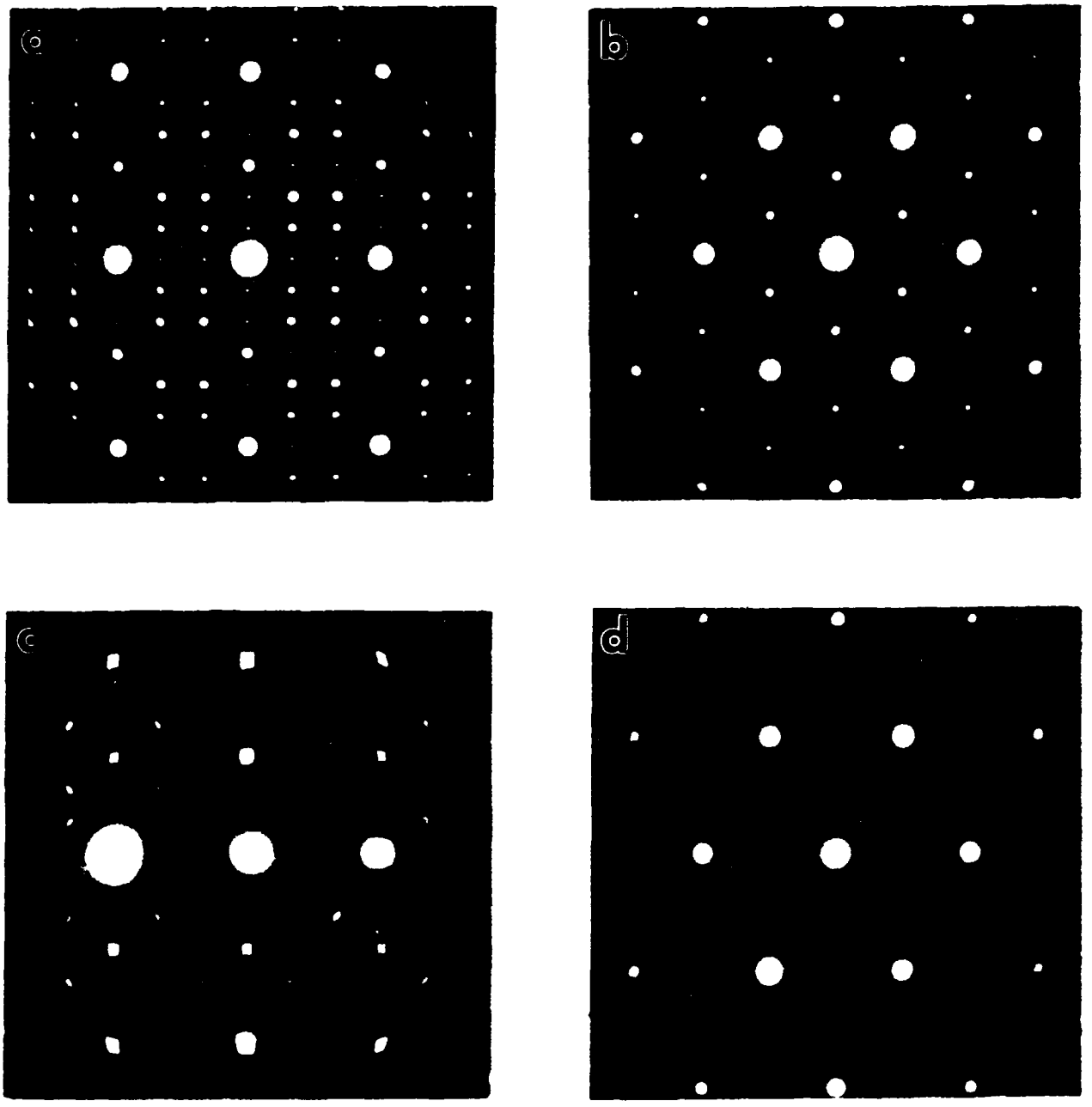

Fig. 2. SADP's from decomposed B2 phase of composition Ti_4Al_3Nb. (a,b) cooled from 1400°C at ~400°C/min. (c,d) water-quenched from 1100°C.

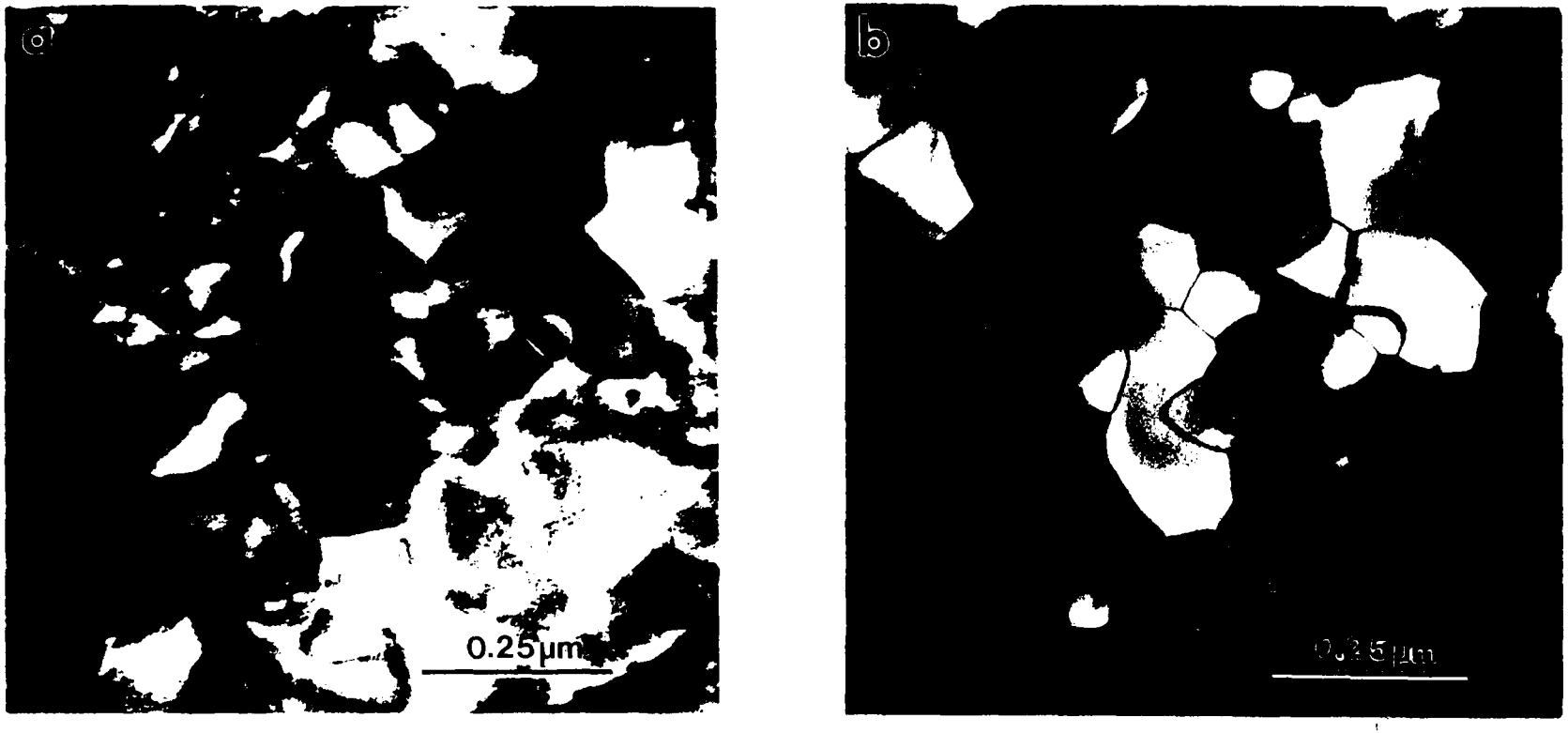

Fig. 3. Microstructure of alloy cooled from 1400°C. TEM. (a) Bright-field, (b) dark-field of one rotational variant.

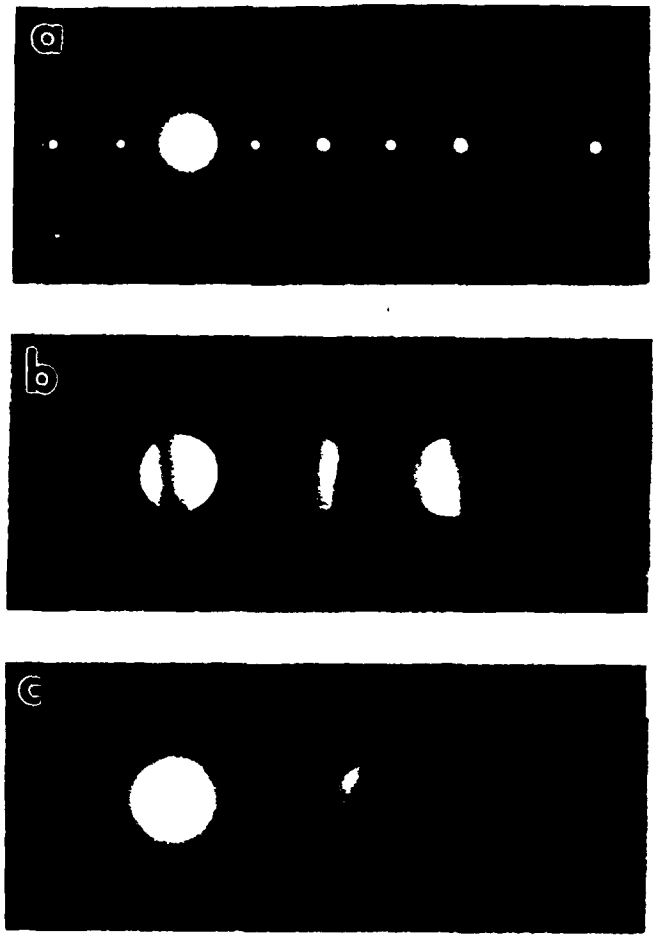

Fig. 4. Single row excitation showing presence of odd (000ℓ) reflections.

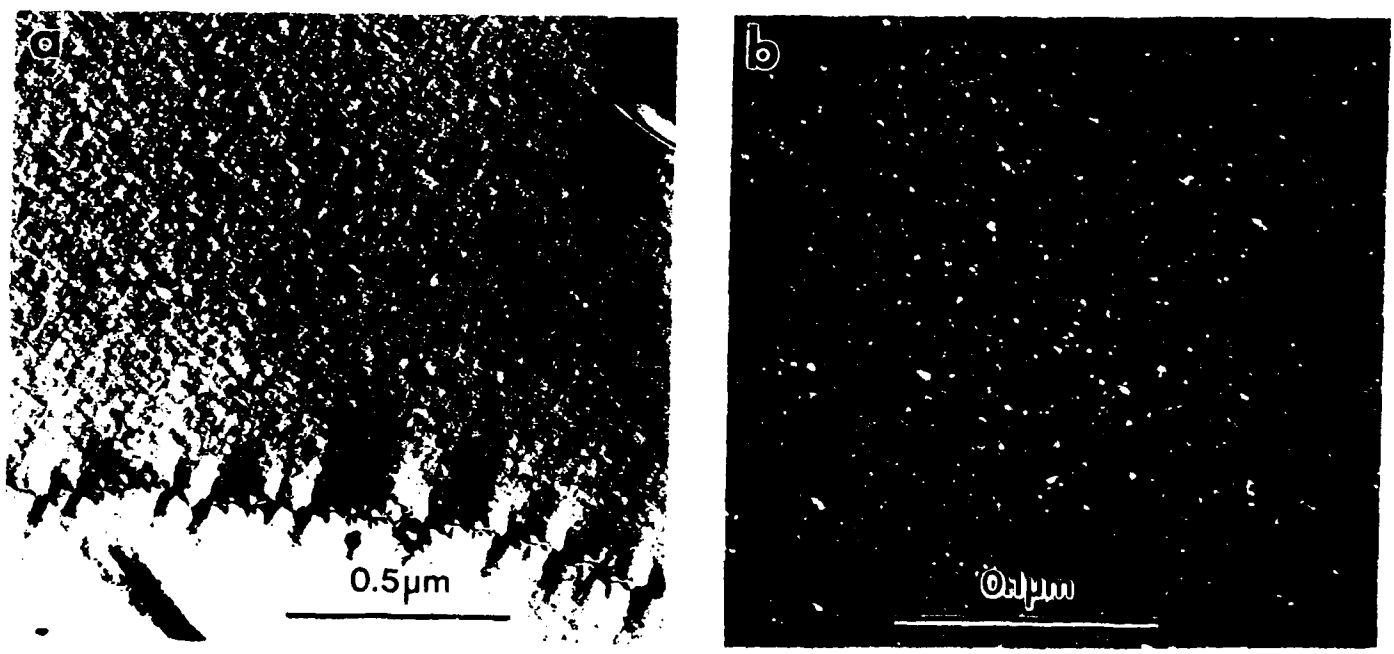

Fig. 5. Microstructure of alloy quenched from 1100°C showing striations and discrete ω-type particles. TEM. SADP's are shown in Fig. 2c and 2d.

Fig. 6. Optical micrograph of alloy annealed at 700°C.

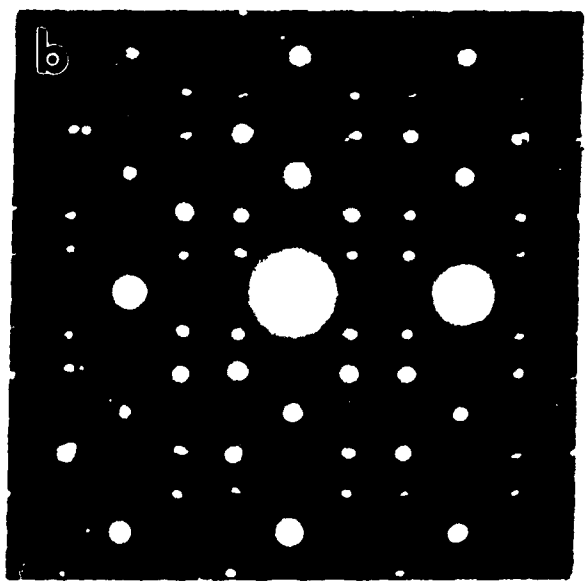

Fig. 7. (a) TEM micrograph of the matrix phase of an alloy annealed at 700°C showing multi-domain structure. (b) SADP.

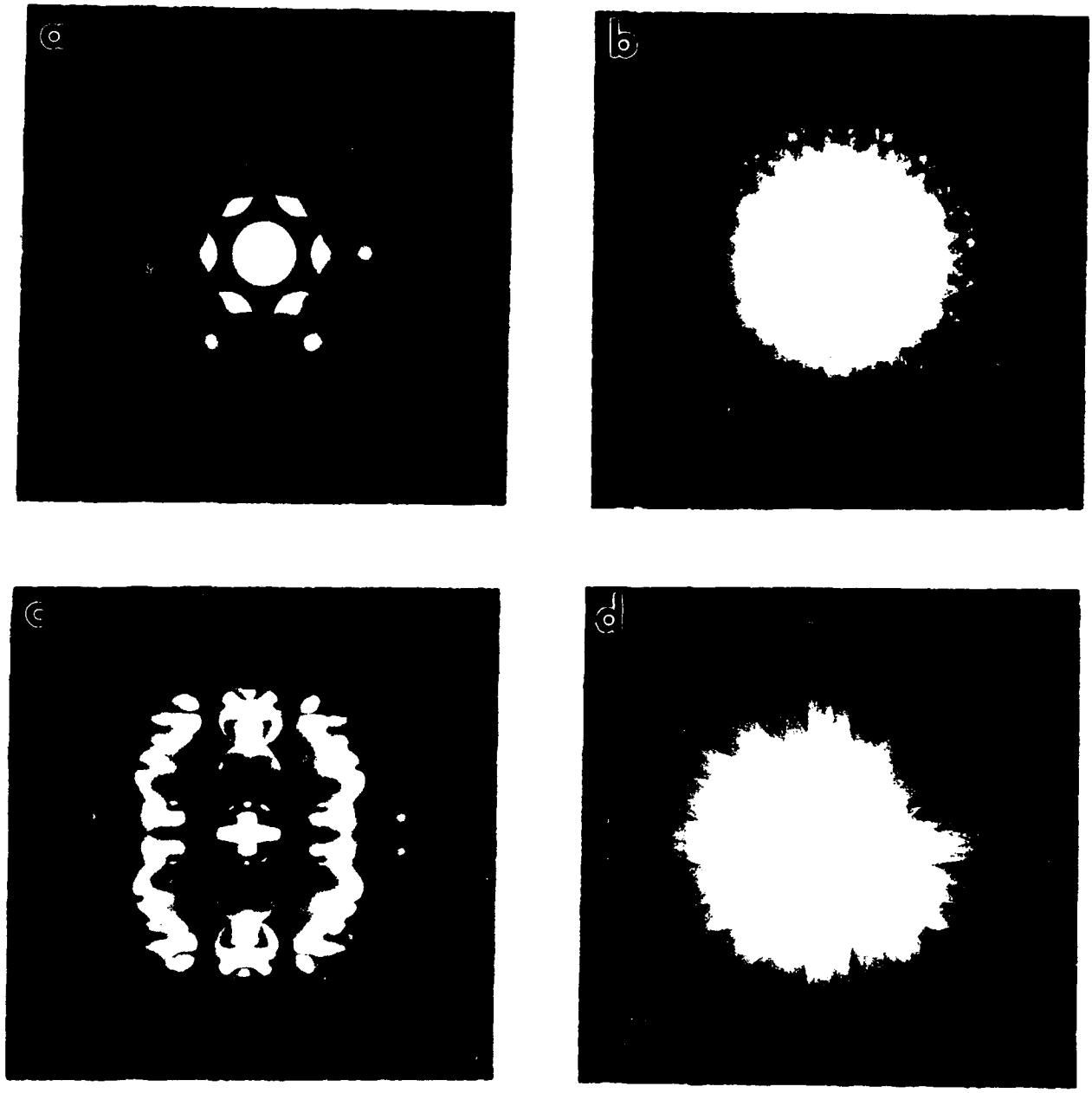

Fig. 8. High (a,c) and low (b,d) magnification CBED patterns in [0001] and [1120] orientations from a single domain of the matrix phase in an alloy annealed at 700°C. The patterns are consistent with point group symmetry 6/mmm.

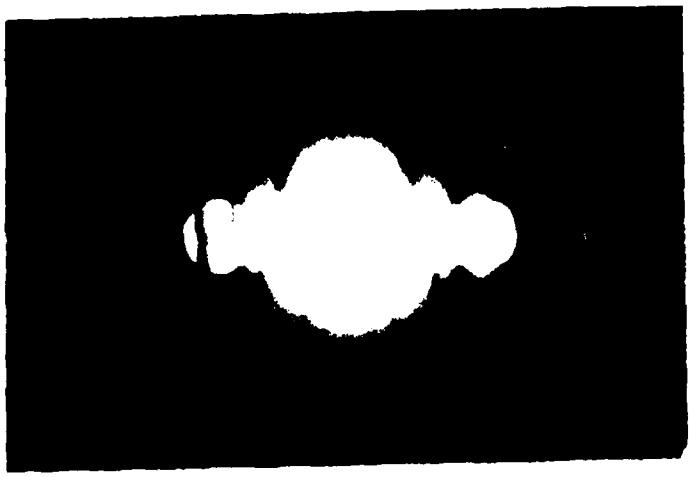

Fig. 9. Single row excitation showing absence of odd (000ℓ) reflections.

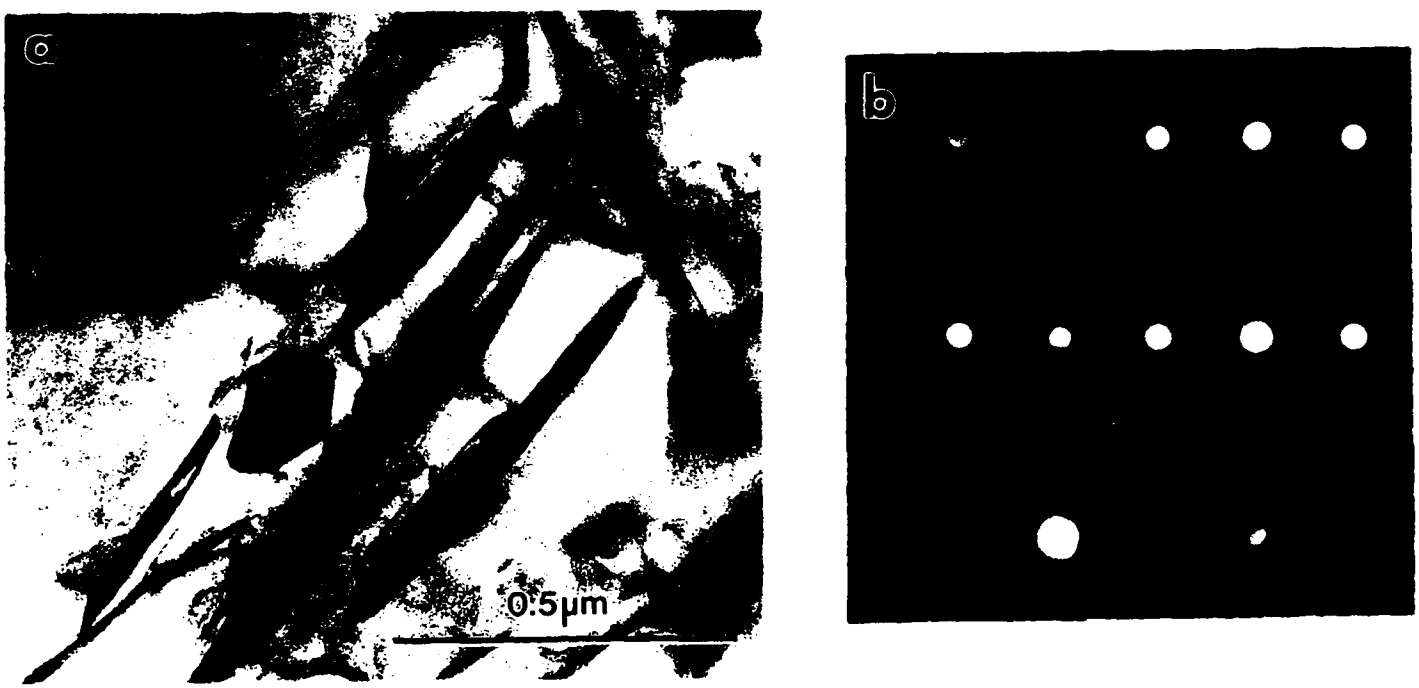

Fig. 10. (a) Needles observed in alloy annealed at 700°C and (b) identified as the $L1_0$ phase.

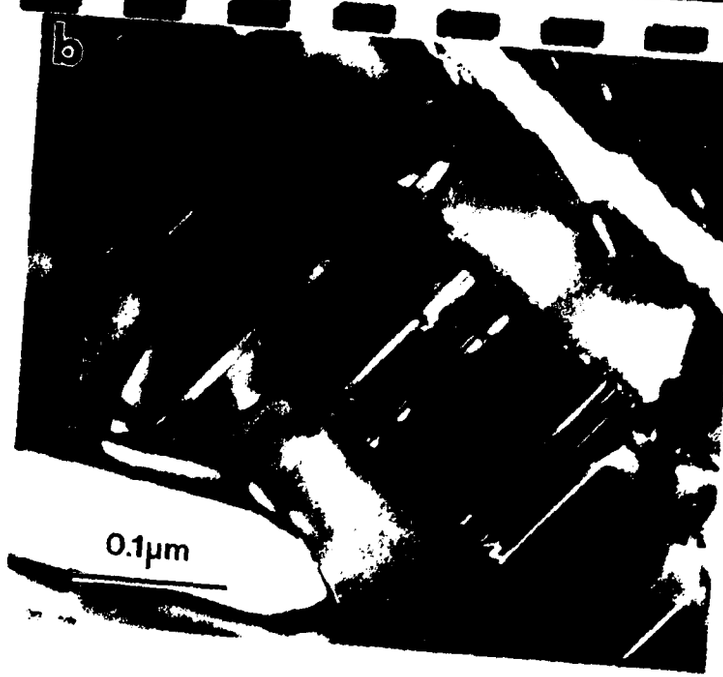

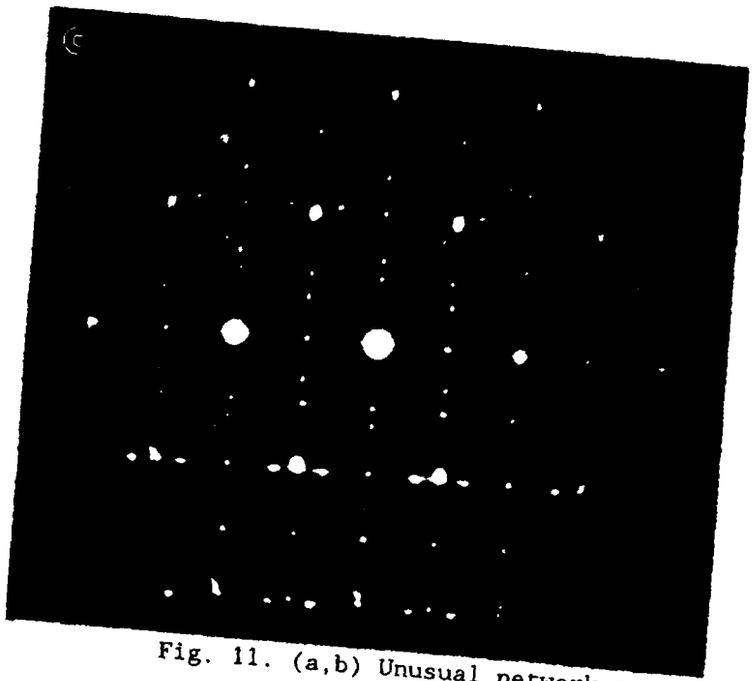

Fig. 11. (a,b) Unusual network structure observed in alloy annealed at 700°C.
(c) SADP showing superposition of $B8_2$, $L1_0$ and DO_{19} phases.

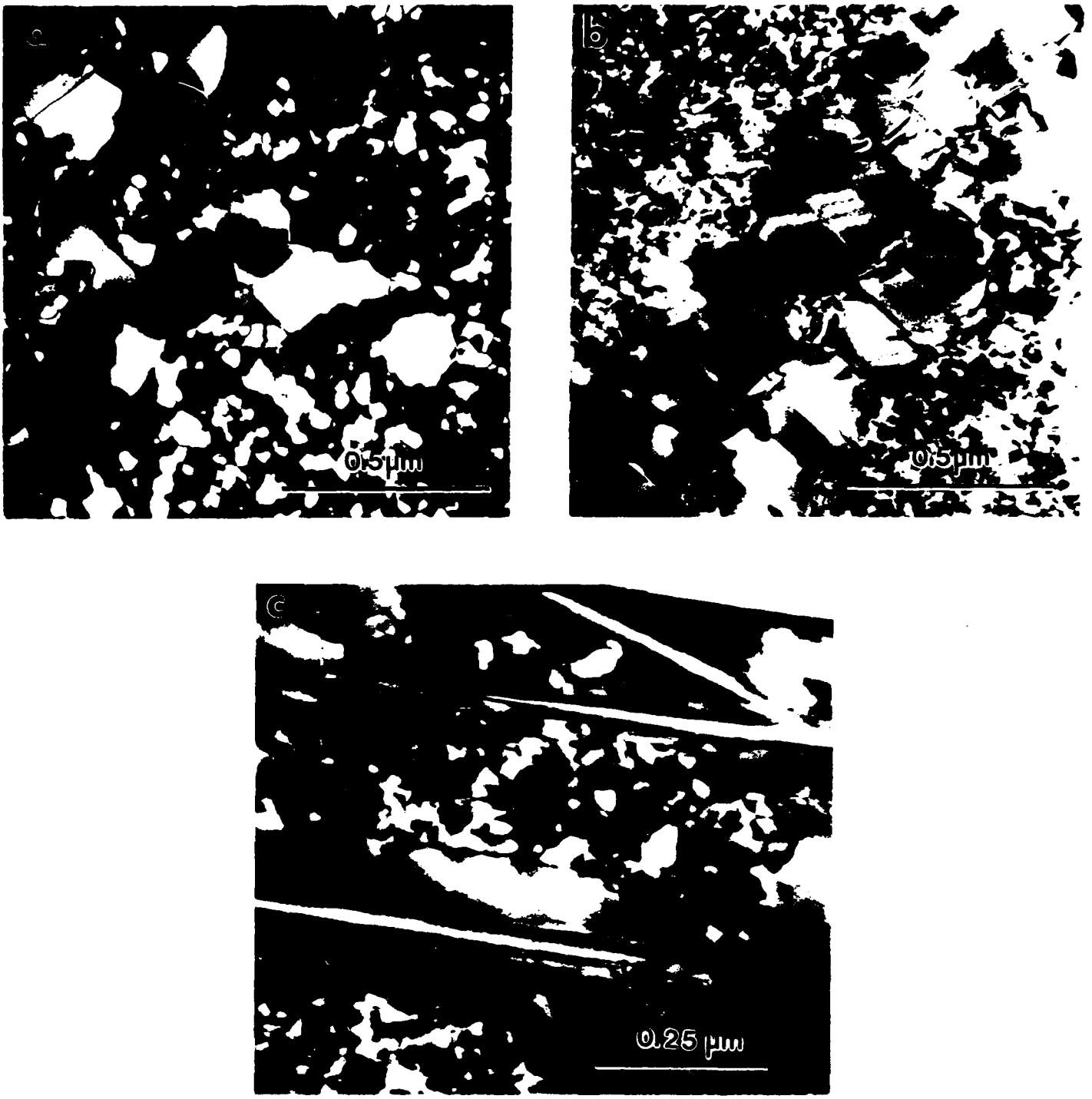

Fig. 12. (a) Large $B8_2$ domains adjacent to fine ω'' domains. (b) Formation of $B8_2$ domains along an unidentified heterogeneity and (c) along a plate of the $L1_0$ phase.

INDENTATION TESTING OF Ti-Al-Nb ALLOYS

1100 C - 4 DAYS

Ti-25Al-12.5Nb
275 VHN - NC

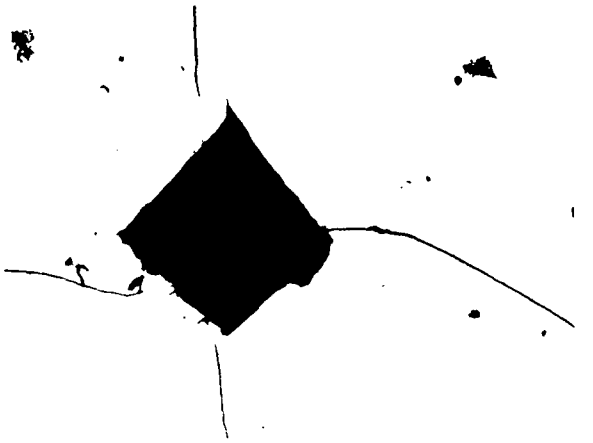

Ti-37.5Al-12.5Nb
331 VNH - KC=0

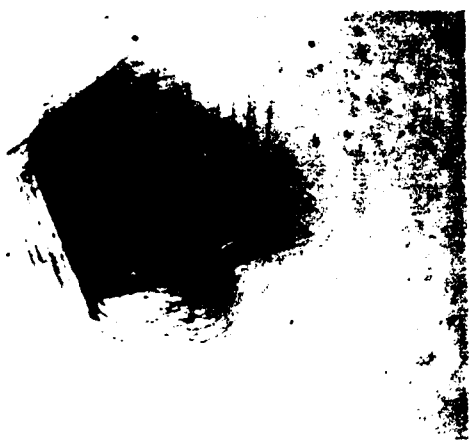

Ti-25Al-25Nb
315 VNH - NC

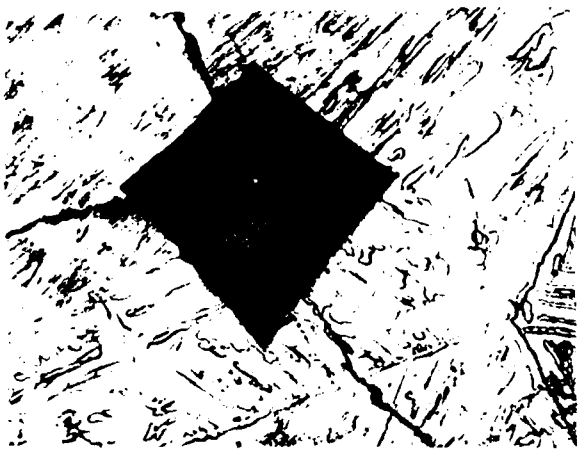

Ti-25Al-37.5Nb
366 VNH - KC≅5

Ti-12.5Al-37.5Nb
214 VNH - NC

Fig. 13. 120 Kg hardness impressions in Ti-Al-Nb Alloys of the indicated compositions which were heat treated at 1100°C for 4 days.

Ti_2AlNb INDENTATION TESTING

120 Kg LOAD

EFFECT OF HEAT TREATMENT

1400 C 3 HRS

171 VHN - NC

1100 C 4 DAYS

315 VNH - NC

850 C 1 DAY

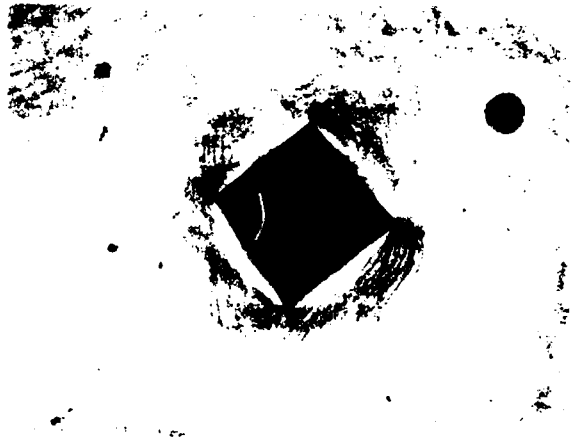

454 VNH - NC

Fig. 14. 120 Kg hardness impressions in Ti_2AlNb with the indicated heat treatments. The samples did not crack and the scale of slip has been refined by the low temoerature heat treatment.

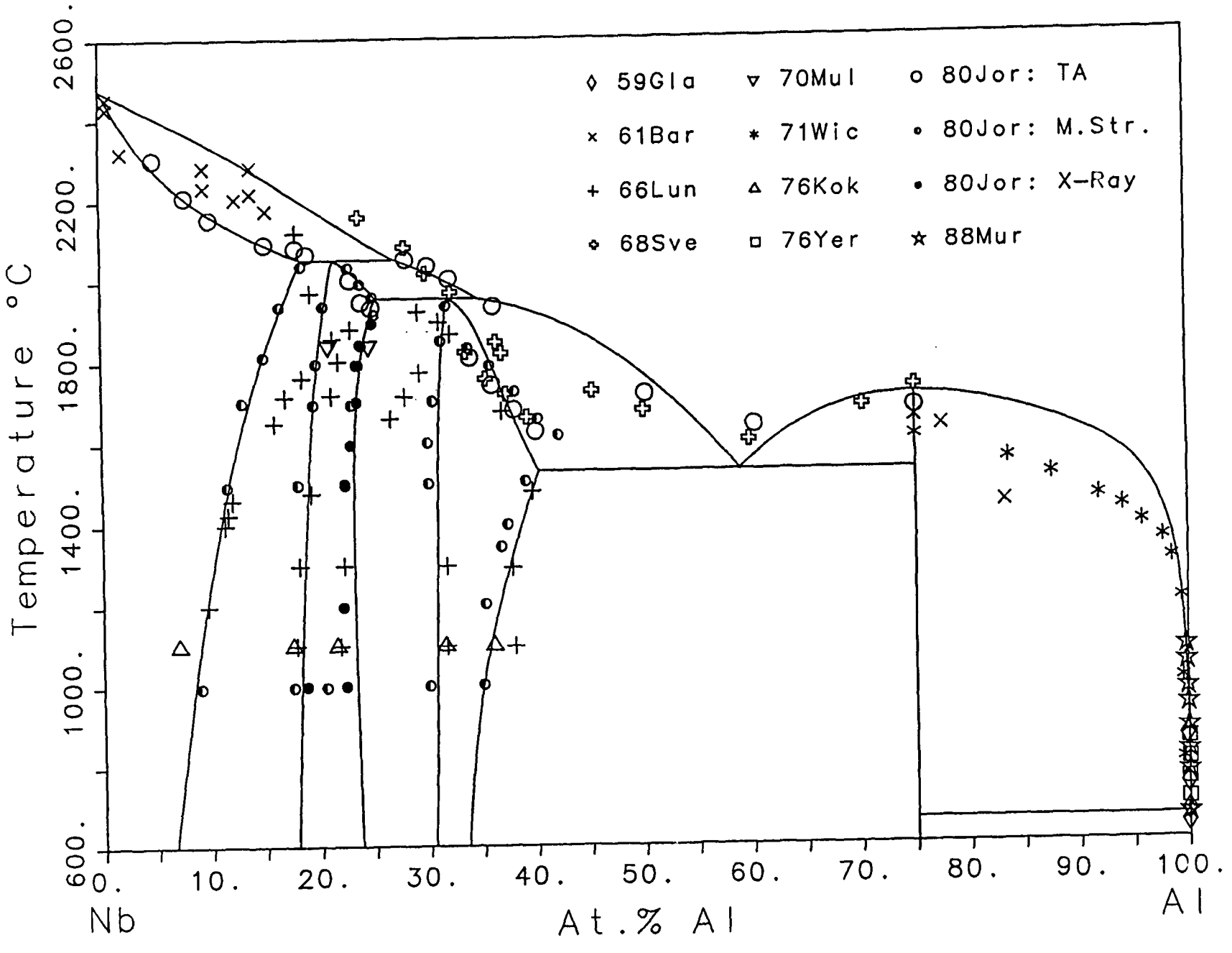

Fig.15. Calculated and measured phase diagram of the Nb-Al system.

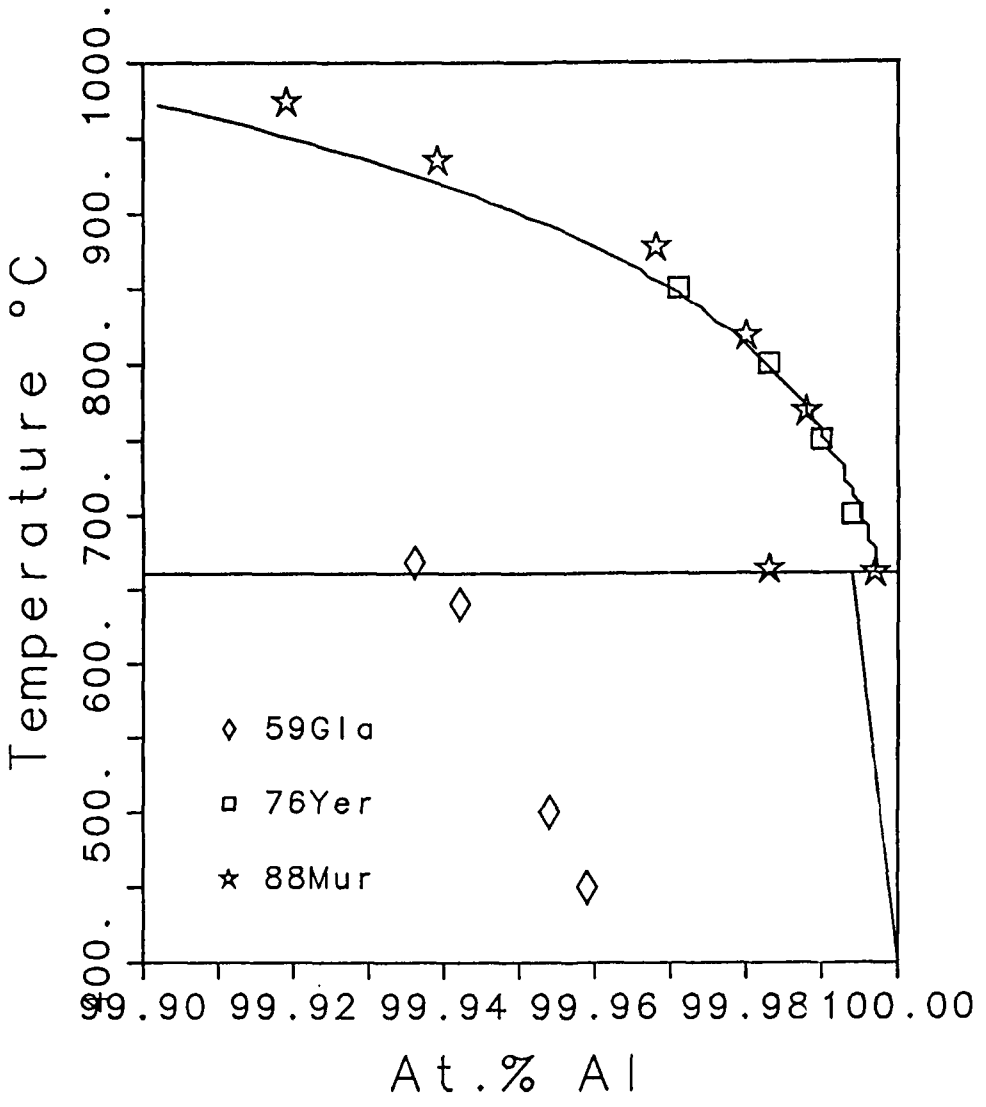

Fig.16. Calculated and measured Al-rich part of the Nb-Al phase diagram.

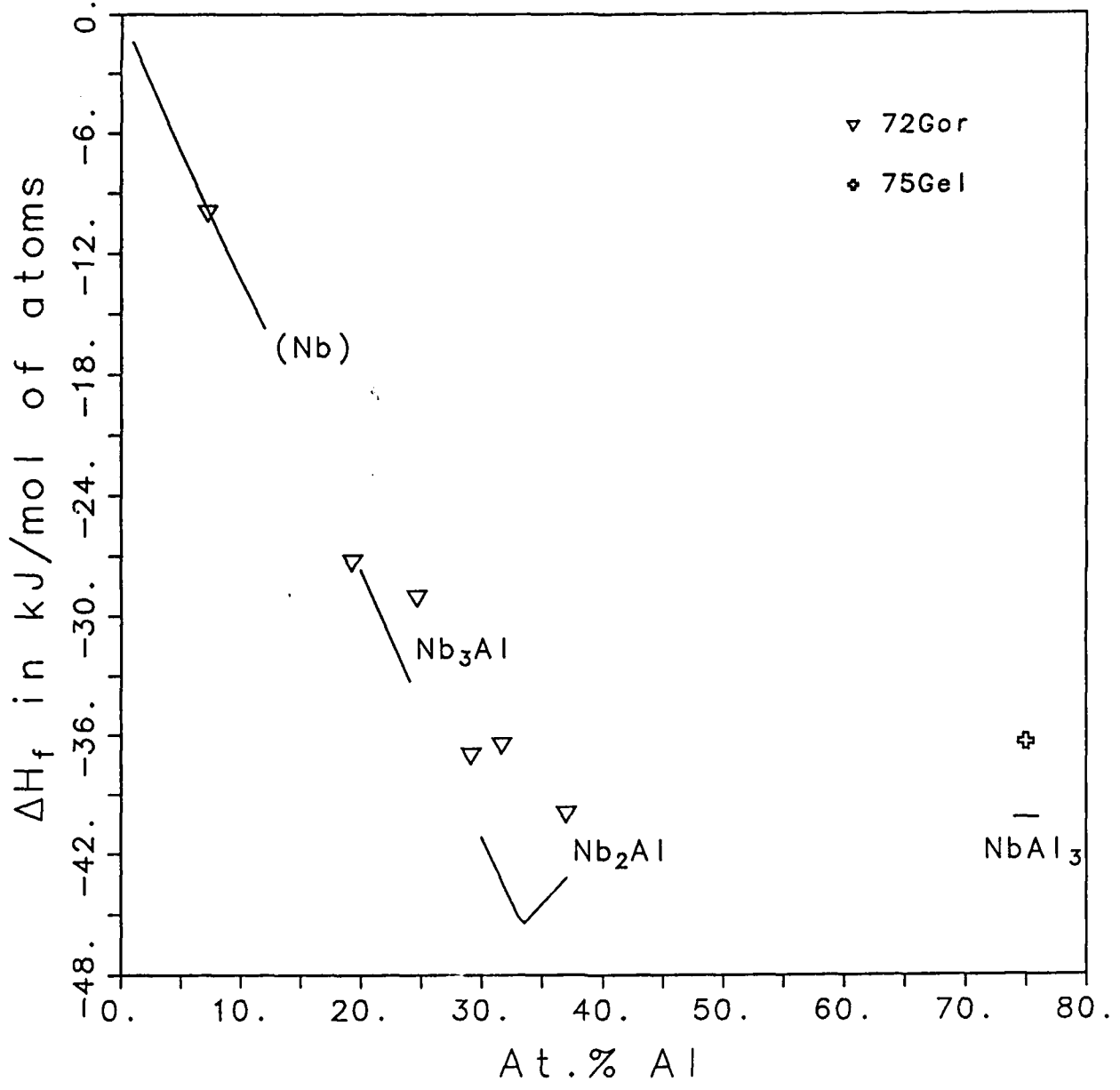

Fig.17. Calculated and measured enthalpies of formation of the solid phases at 25 °C.

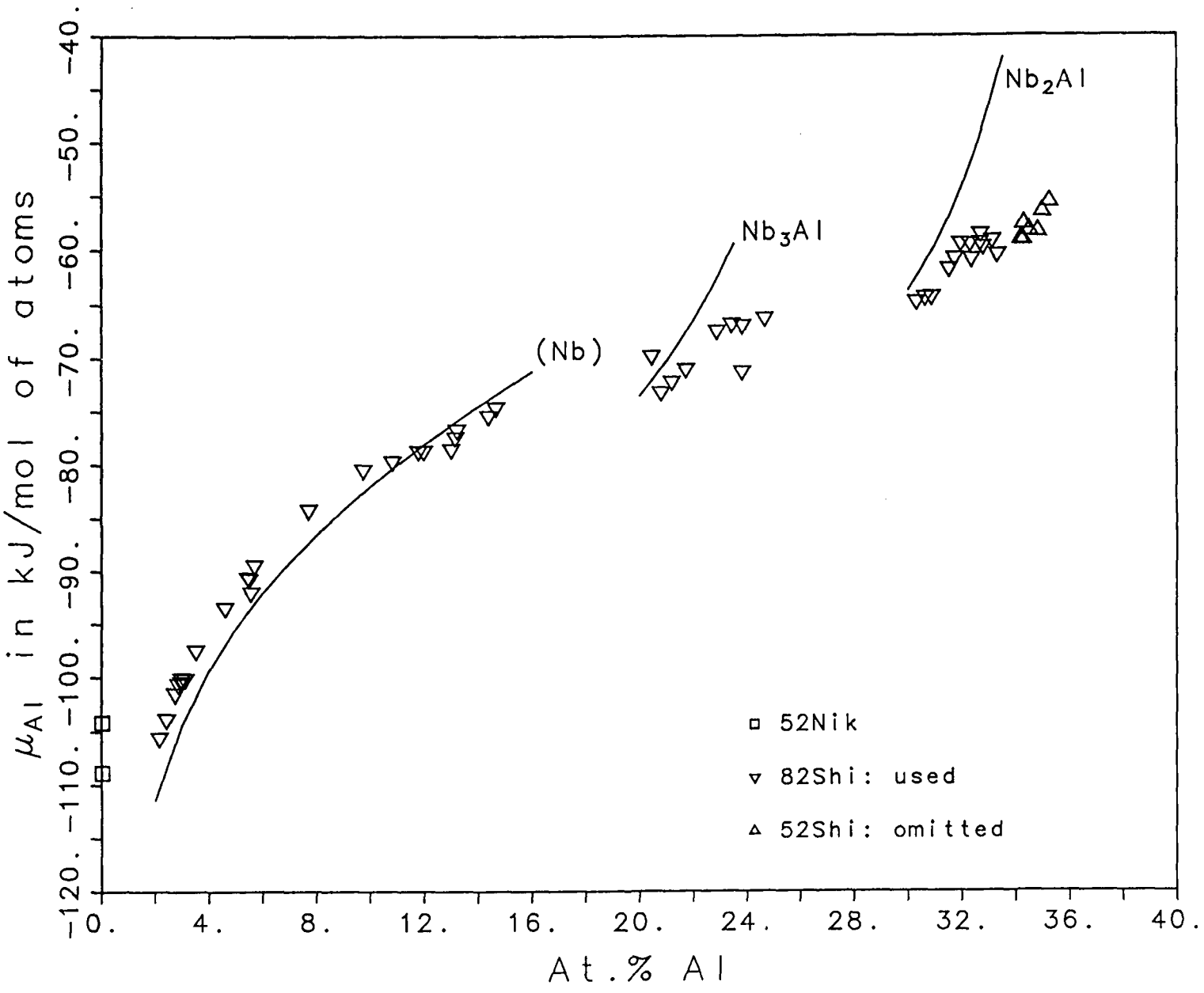

Fig.18. Calculated and measured partial Gibbs energies of Al in the solid phases at 1727 °C (2000 K).

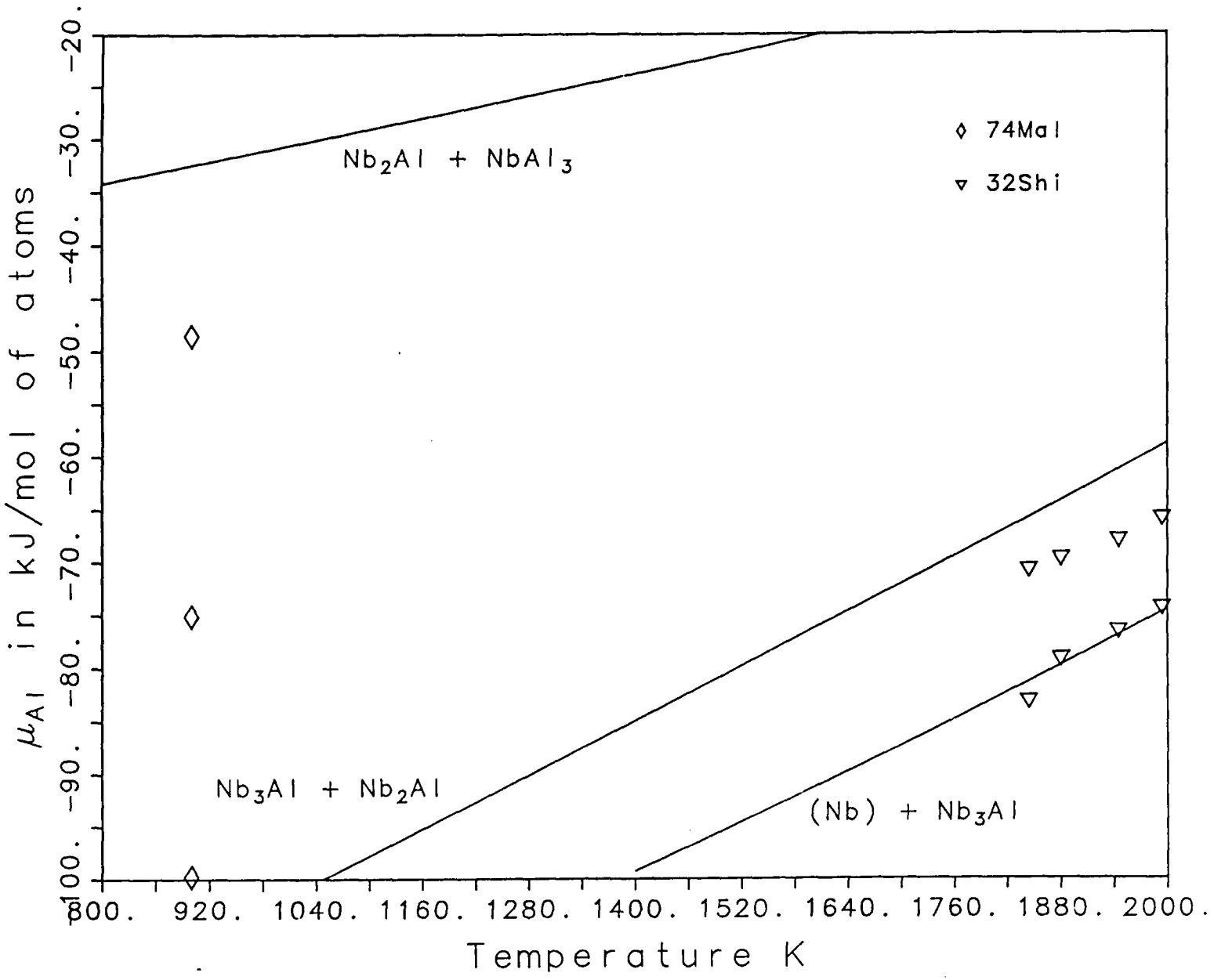

Fig.19 Calculated and measured partial Gibbs energies of Al in the two-phase equilibria of the solid phases.

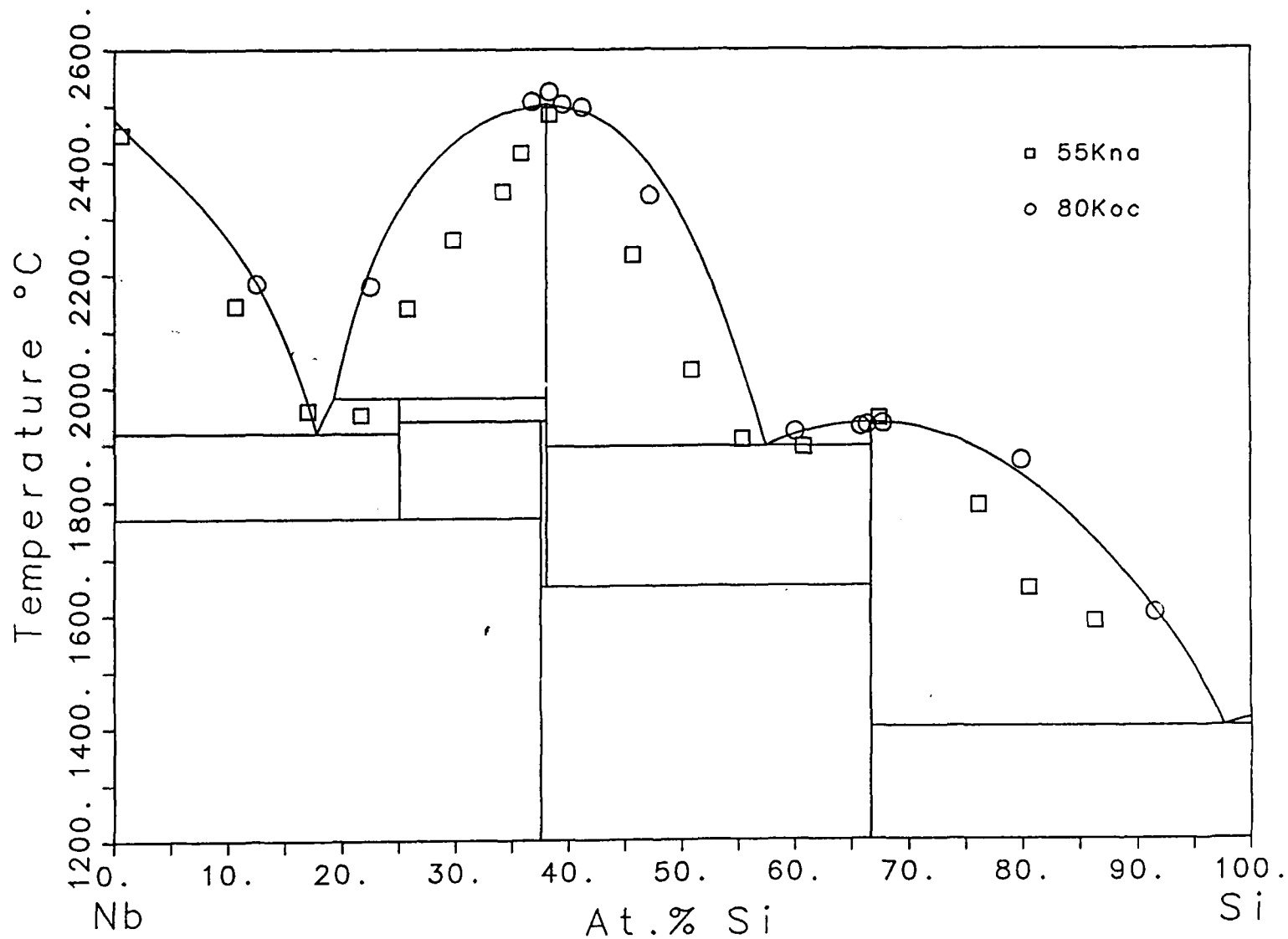

Fig.20 Calculated and measured phase diagram of the Nb-Si system.

APPENDIX

OMEGA-RELATED PHASES IN A Ti-Al-Nb ALLOY

Leonid A. Bendersky and William J. Boettinger

Metallurgy Division, National Institute of Standards and Technology, Gaithersburg, MD 20899

Study of phase equilibria in the Ti-Al-Nb system is often complicated by the possibility of rapid ordering reactions of a chemical or displacive type during cooling from high temperatures. In the present study we have investigated the decomposition of the high temperature B2 phase of composition Ti-37.5at%Al-12.5at%Nb into "omega-type" phases during either cooling or low temperature annealing. Formation of an "omega-type" phase from the high temperature B2 matrix of composition Ti-27.8at%Al-11.7at%Nb was observed previously by [1]. If the "omega-type" phase forms by pure displacive ordering, i.e. by collapse of (111) plane pairs of the B2 phase, the resulting structure will be as shown in Fig.1a (termed ω'). The chemical order of the ω' phase is directly inherited from the B2 structure. The space group of the ω' phase is P3m1 (#164). The same authors [1] suggested a secondary transformation of the ω' phase to another omega-type phase with the $B8_2$ structure shown in Fig.1b. The space group for the $B8_2$ structure is hexagonal $P6_3/mmc$ (#194) with reflection conditions such that the 1100 reflection is present, but the 0001 (or $000\ell, \ell=2n+1$) is absent.

This note confirms the presence of the phase with the $B8_2$ structure as an equilibrium low temperature phase using convergent beam electron diffraction (CBED). However the mechanism of the low temperature decomposition of the B2 phase is more complex than was suggested by Strychor et al. [1]; viz., an intermediate trigonal phase, ω'' is formed with a structure shown in Fig.1c.

Fig.2a,b show convergent beam electron diffraction (CBED) patterns of an omega-type phase annealed at 700 C for one month. The whole pattern symmetry is 6mm for the [0001] orientation and 2mm for the $[11\bar{2}0]$ orientation. These whole pattern symmetries determine unambiguously that the phase has hexagonal point group symmetry 6/mmm (see tables in [2]). The absence of odd 000ℓ reflections in a diffraction condition obtained by exciting only one row suggests that they are kinematically forbidden. Observation of dynamic extinction in a kinematically forbidden 0001 reflection in the form of a black cross (Fig.2b) for the $[11\bar{2}0]$ zone axis, (a result of the simultaneous presence of a screw axis and a glide plane) can be explained only by the space group $P6_3/mmc$. This result seems to suggest the existence of an equilibrium low temperature TiAlNb $B8_2$ phase (in equilibrium with DO19 and $L1_0$ phases, as will be shown elsewhere [3]).

All specimens cooled from high temperature go through a rapid phase transformation during cooling from the B2 to a different "omega-type" phase. The phase has selected area diffraction patterns indistingushiable from the $B8_2$ phase (Fig.3). Using microdiffraction it was shown that odd 000ℓ reflections are present (Fig.4). The same is true for all hh00 reflections. Therefore, the phase has neither the $B8_2$ nor the ω' structure. The diffraction data fits the proposed ternary ω'' phase shown on Fig.1c. X-ray single crystal diffraction results seem to confirm this [3].

ACKNOWLEDGEMENT

The support of the DARPA under Order #6065 is appreciated.

REFERENCES

1.R.Strychor, J.C.Williams and W.A.Soffa, Met.Trans., 19A, 225 (1988).
2.B.F.Buxton, J.A.Eades, J.W.Steeds and G.M.Rackham, Phil.Trans., 281, 171 (1976).
3.L.A.Bendersky, W.J.Boettinger and C.B.Shoemaker, to be published.

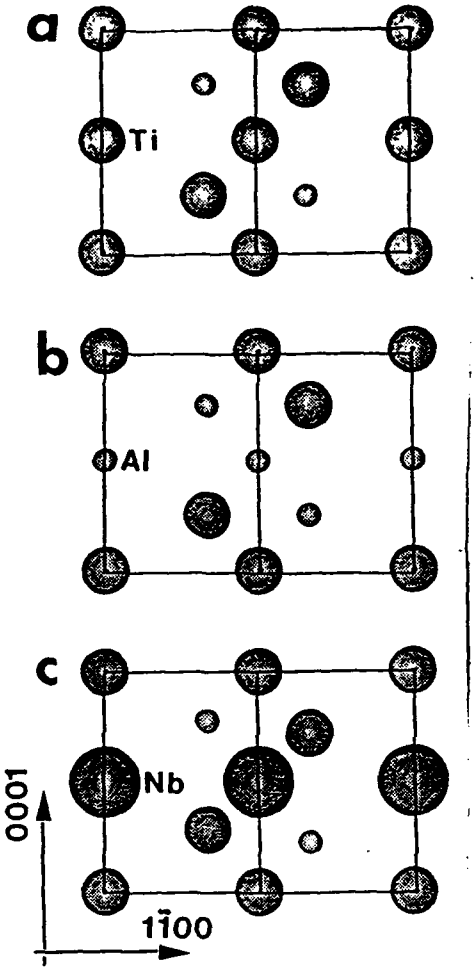

Fig.1 Projected structure of one hexagonal unit cell of the ω'(a); $B8_2$(b); ω''(c) phases in the [11$\bar{2}$0] direction.

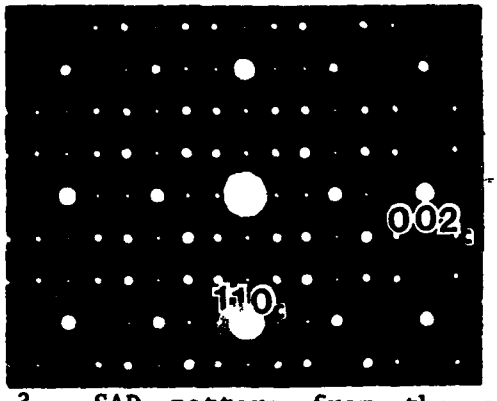

Fig.3 SAD pattern from the cooled specimen at $\langle 110 \rangle_{cub}$ orientation. The same pattern was observed for the annealed specimen.

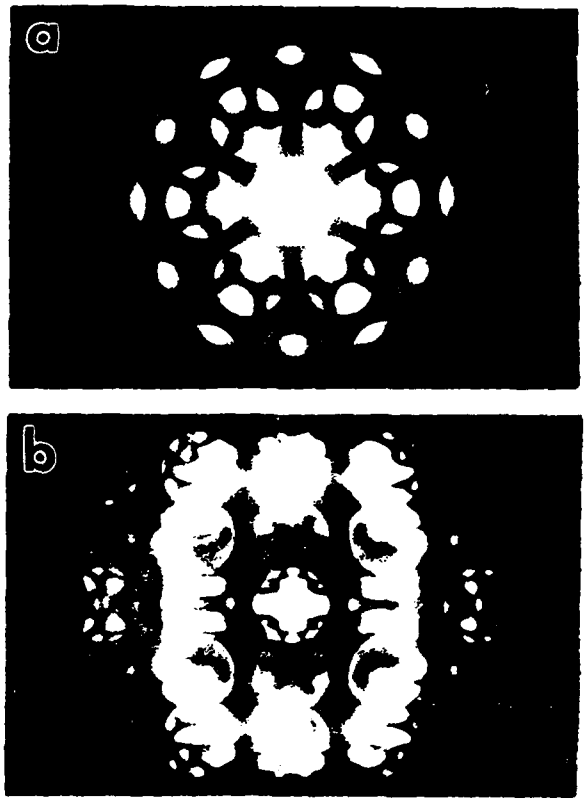

Fig.2 CBED patterns at [0001] (a) and [11$\bar{2}$0] (b) zone axis orientations of an annealed specimen. The $P6_3/mmc$ space group of $B8_2$ structure can be derived.

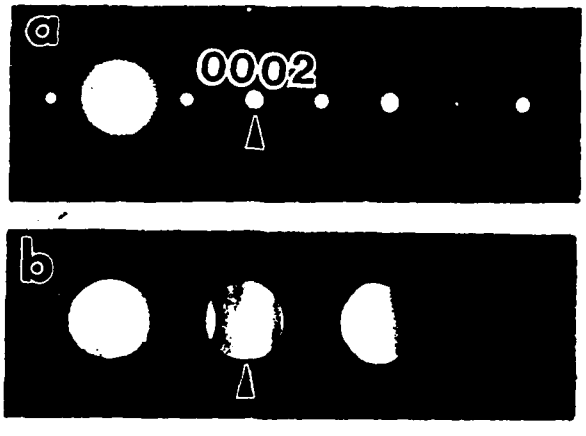

Fig.4 SAD(a) and CBED(b) patterns of a row of 000l reflections showing the presence of odd reflections for the cooled specimen.

INVESTIGATION OF B2 AND RELATED PHASES IN THE Ti-Al-Nb TERNARY SYSTEM

LEONID A. BENDERSKY AND WILLIAM J. BOETTINGER
Metallurgy Division, National Institute of Standards and Technology, Gaithersburg, MD 20899, USA

ABSTRACT

Alloy compositions around Ti_2AlNb were studied to establish phase equilibria and transformations during cooling from 1100°C and 1400°C. In addition to general results obtained on a wide range of compositions, which include evidence for a broad B2 phase field, transformation of BCC Ti_4Al_3Nb to a phase with an omega-type structure is reported. Detailed analysis indicates that this phase has the $B8_2$ structure after annealing at 700°C.

INTRODUCTION

Titanium aluminides (Ti_3Al and TiAl) with Nb additions have received considerable attention as potential low density, high strength and creep-resistant materials for high temperature application. Because the presence of BCC and BCC-related phases in these alloys seems to have an important role in their mechanical properties, in-depth studies of the BCC phase field are necessary. Surprisingly, the phase equilibria in this ternary system are poorly understood. The only detailed studies are for alloys of Ti_3Al with Nb substitution for Ti up to 20 at% by Strychor et al.[1] and Banerjee et al. [2,3]. Both show the existence of a high temperature BCC or B2 phase which generally transforms during cooling to an ordered hexagonal DO_{19} phase. The variety of observed microstructures reported shows extreme sensitivity of the alloys to the details of heat treatment. Probably because of this, the two studies have reported quite different results. Banerjee et al.[3] found that upon slow cooling both B2 and DO_{19} phases transform partially to an orthorhombic phase with symmetry Cmcm. They suggest a structural relationship between this phase and the hexagonal DO_{19} phase. No such phase was observed by Strychor et al. [1]. Instead, an ordered omega phase was observed. The phase precipitates from the retained B2 phase during low temperature annealing. Arguments about further transformation of the omega phase to a $B8_2$ (Zr_2Al) phase were also presented.

Recently we have begun an experimental study on phase equilibria and phase transformations in the ternary Ti-Al-Nb system. In order to cover a wide range of compositions, five different alloys including and surrounding Ti_2AlNb were chosen for study. In this paper we present preliminary results on possible equilibrium phases at 1400°C and 1100°C for these alloys. The focus of the paper is on the alloy with the Ti_4Al_3Nb composition for which a complex transformation of BCC to an omega-type structure was observed.

EXPERIMENTAL PROCEDURE

Alloys with compositions Ti_5Al_2Nb(alloy #3), Ti_2AlNb(#30), Ti_4Al_3Nb(#4), $Ti_3Al_2Nb_3$(#2) and Ti_4AlNb_3(#1) were prepared by arc melting. In excess of ten remelts were necessary to ensure mixing of the components. Cast buttons were homogenized at 1400°C for three hours in a furnace under 2/3 atm gettered Ar. It was found necessary to rest the samples on a Y_2O_3 coated Al_2O_3 substrate to prevent reaction with Al_2O_3. Heat treatments at 1100°C for 4 days were performed after the 1400°C treatment by lowering the furnace temperature. Cooling to room temperature was performed by lowering the samples out of the hot zone of the furnace into a lower chamber. The cooling rate was estimated to be about 400°C/min.

RESULTS

Microstructure of Samples Heat Treated at 1400°C

Optical metallography of all samples cooled from 1400°C reveals the elimination of the dendritic microsegregation of the cast structure and the presence of very coarse grains (~2 mm) of an apparent single phase. As TEM examination shows, however, the high temperature phase is transformed to other phases during cooling. The resultant microstructures are fine and not resolved by optical metallography except for alloy #3.

For alloy #3 (Fig.1a) the microstructure consists of a martensite-type morphology with plates of the DO_{19} phase related to each other by the Burgers orientation relationship. This microstructure is well known for Ti alloys [1] and indicates a transformation from the high temperature BCC phase to the DO_{19} phase during cooling. The presence of a high density of APBs (anti-phase boundaries) in the DO_{19} phase suggests that the first step of the transformation was the formation of the disordered hexagonal phase.

For alloy #30 the microstructure consists of a B2 matrix phase with a small fraction transformed to polydomain plates of the DO_{19} phase (Fig.1b). The microstructure appears similar to the initial stage of the same transformation for the #3 alloy. The BCC phase has B2 ordering and strong diffuse streaking along 110 directions (Fig.2a). No APBs due to the B2 ordering were observed. In two-beam imaging the matrix shows strain contrast referred to in the literature as "tweed"[1].

Alloy #2 has large grains of the B2 phase showing diffraction effects similar qualitatively to that of the alloy #30 matrix. No APBs due to the BCC/B2 ordering or other phases were observed.

Alloy #1 also has a single phase B2 microstructure. The only difference compared to the #2 and #30 alloys is that the B2 ordering reflections are noticeably weaker (Fig.2b).

Alloy #4 has a microstructure consisting of small (~0.2 μm) domains (Fig.3a) which are clearly the result of solid state transformation from a high temperature BCC (or B2) phase during cooling. Selected area diffraction with a large aperture from a large number of domains shows patterns with strong fundamental and superlattice reflections of the B2 phase - e.g. <110> and <111> cubic orientations in Fig.4a,b. Reflections in addition to those of the B2 phase can be identified as belonging to four rotational domains of an omega phase (hexagonal Bravais lattice: a=0.46 nm, c=0.58 nm) with $\langle 111\rangle_{bcc}//[0001]_h$ and $(110)_{bcc}//(1120)_h$. The omega phase is ordered and has a "c" parameter twice that of the disordered phase. This transformation will be discussed in more detail in the Discussion.

Microstructure of Samples Heat Treated at 1100°C

The microstructure of samples cooled from a 4 day heat treatment at 1100°C observed by optical metallography show that specimens #3, 30 and 1 are in a single phase region at 1100°C. According to TEM observation, the phase is similar to that at 1400°C. For the other two specimens, #2 and 4, precipitates coarse enough to be considered at equilibrium at 1100°C were observed. The second phases were identified by electron diffraction as the sigma phase (tetragonal $AlNb_2$) for specimen #2, and the DO_{19} phase (hexagonal Ti_3Al) for specimen #4. The compositions of these phases and the matrix were measured by SEM microprobe and shown by the tie-lines in Fig.5b. According to TEM observation, the matrix phases are similar to those observed for the 1400°C annealed alloys.

DISCUSSION

According to the results presented in the previous section, the BCC or B2 phase is the high temperature phase at both 1400°C and 1100°C. Fig.5 shows the estimated single phase field of this phase for the temperatures studied using our data and the general shape of the BCC field obtained from preliminary thermodynamic calculation of the Ti-Al-Nb ternary diagram [4]. For all five alloys, B2 order can not be ruled out at temperature. For alloys #1, 2 and 30 the ordered B2 phase was observed after cooling. Since no APBs from B2 ordering were observed for these specimens, it is possible that the B2 phase is an equilibrium phase at both temperatures. We have thus sketched a region of the BCC field in which B2 order exists in Fig.5. However it is also possible that the APBs were annealed out during the relatively slow cooling in our experiments, and the ordering temperature is lower than 1100°C. Estimates of the antiphase domain coarsening rate are too slow to support this conjecture. High cooling rate quenching or high temperature X-ray diffraction experiments are now in progress to establish the ordering temperature.

For the composition of alloy #3, the equilibrium phases at 1100°C have been reported as B2 and DO_{19} [3]. Our results suggest that the equilibrium is single phase BCC. In our alloy #3 the DO_{19} phase forms only during cooling from 1100°C and has a high density of APBs. The transformation path is thus BCC to hex.(disord.) to DO_{19}. Our results also suggest that the BCC/B2 ordering only occurs in the absence of the BCC to HEX transformation and thus is metastable at this composition and occurs below 1100°C. Possibly small differences in composition or heat treatment temperature may have caused our discrepancy with [3].

For alloy #4 the following arguments about the nature of BCC phase ordering and phase transformation could be applied. According to Strychor et al. [1], the B2 phase transforms by collapse of (111) planes to the ordered omega phase which subsequently orders to the hexagonal $B8_2$ phase (actually it is disordering since the space group of the $B8_2$ ($P6_3/mmc$) is a supergroup of the omega phase(P3m1)). The arguments of [1] are based on the presence of 1100 reflections of omega at $1/3\langle 112\rangle_{bcc}$ which have zero structure factor for both the ordered and disordered omega phase. These reflections are also observed for our alloy #4 (see Fig.4b). Dark-field imaging with the 1100 reflection shows only one rotational variant which includes three translational variants separated by well-imaged interfaces (Fig.3). No BCC or B2 phase was observed between the domains. The dark-field imaging plus tilting to an orientation where only a hh00 row of reflections is excited shows that the observed non-zero 1100 structure factor is not the result of double diffraction.

However the 1100 reflection is not forbidden by the P3m1 space group symmetry [5], and has zero structure factor only for particular states of order inherited from the BCC or B2. Deviations from that order (e.g. different occupancy on sites 1b and 2d) will change the 1100 structure factor to non-zero. An example can be a ternary structure of the Ti_3Al_2Nb stoichiometry with Ti on 1a and 2d, Nb on 1b and Al on 2d sites. Therefore information additional to that presented by [1] is required to confirm the existence of the $B8_2$ structure in the Ti-Al-Nb system. For this purpose, convergent beam electron diffraction (CBED) could be used in order to distinguish between the P3m1 and the $P6_3/mmc$ (of the $B8_2$ phase) space groups. This was applied for alloy #4 which was annealed for 26 days at 700°C to produce domains large enough for good CBED. Results from a single domain show that the [0001] zone axis has the 6mm whole pattern symmetry, and that the [1120] zone axis has the 2mm whole pattern symmetry (Fig.6). These results are in agreement with the hexagonal $P6_3/mmc$ space group of the $B8_2$ phase rather than with the trigonal P3m1 space group (for this group for the same zone axes the whole pattern symmetry is 3m and 2, respectively [6]). Additional confirmation of this result was obtained by showing that the 0001 reflection is kinematically forbidden. This was shown by tilting along the 000ℓ row and observation of the disappearance of 000ℓ (with odd ℓ) reflections.

CONCLUSIONS

1. A large BCC phase field was confirmed to exist at 1100°C and 1400°C.
2. B2 order was found for a large composition range and appears to be the equilibrium at 1100°C and 1400°C.
3. A hexagonal $B8_2$ phase, which is structurally related to ordered omega, is probably a low temperature equilibrium phase (700°C) with composition close to Ti_4Al_3Nb. It is questionable if the formation of athermal omega precedes the BCC to $B8_2$ transformation.
4. The existence of high temperature BCC to B2 ordering for this composition remains an open question.

ACKNOWLEDGEMENT

The support of the Defense Advanced Project Research Agency under Order #6065 is appreciated. We thank F.S.Biancaniello and M. Williams for the alloy and TEM specimen preparation and Dr. A. Shapiro for the microprobe analysis.

REFERENCES

1. R.Strychor, J.C.Williams and W.A.Soffa, Met. Trans., 19A, 225 (1988).
2. D.Banerjee, T.Nandi and A.K.Gogia, Scripta Met., 21, 597 (1987).
3. D.Banerjee, A.K.Gogia, T.K.Nandi and V.A.Joshi, Acta Met., 36, 871 (1988).
4. U.R.Kattner, NIST, Gaithersburg, MD, 1988, unpublished research.
5. Inter. Tables for Cryst., Vol.A, T. Hahn (ed.), D. Reidel Publishing Co., Dodrecht (1987).
6. B.F.Buxton, J.A.Eades, J.W.Steeds and G.M.Rackham, Phil. Trans., 281, 171 (1976).

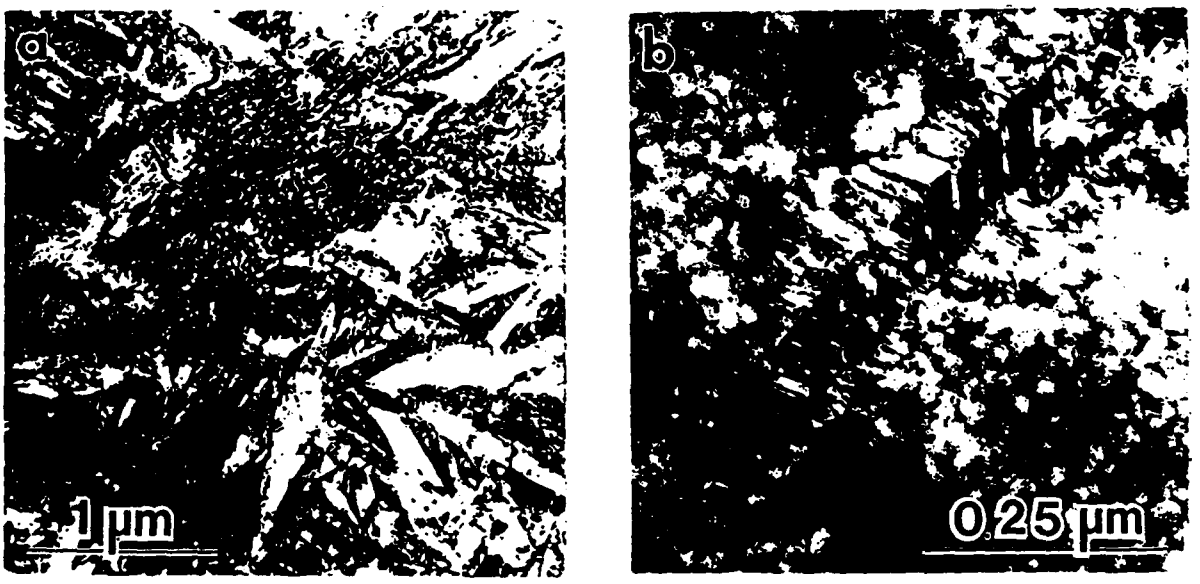

FIG.1 TEM micrographs of the microstructure of specimens cooled from 1400°C temperature. a) alloy #3 with martensite-type morphology of the DO_{19} phase. b). alloy #30 with the B2 phase matrix and a polydomain plate of the DO_{19} phase. Similar microstructures are observed for specimens cooled from 1100°C.

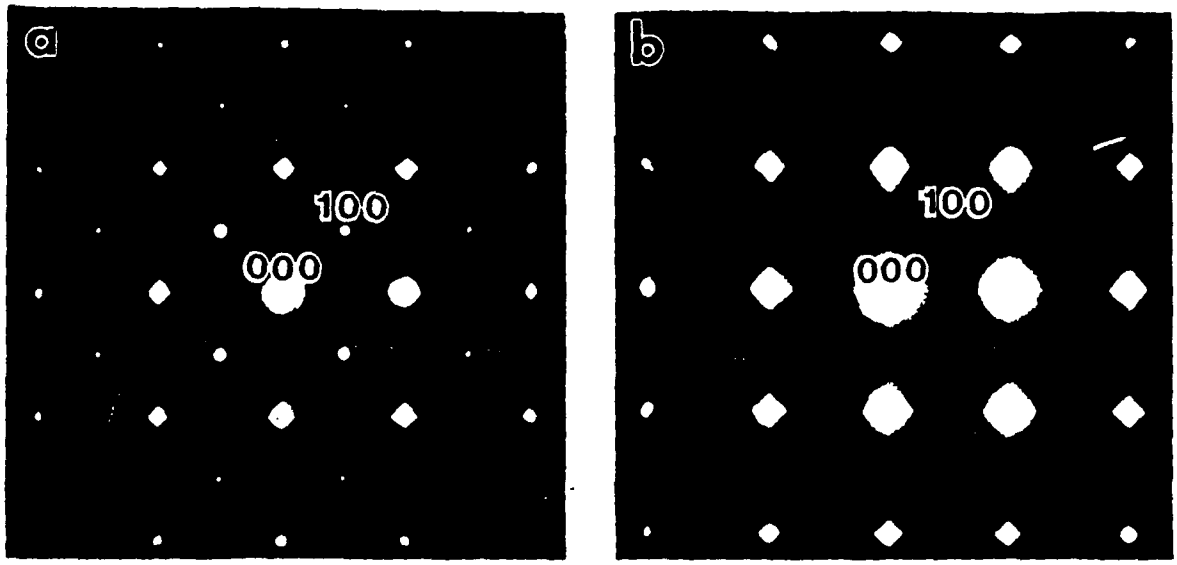

FIG.2 SAD patterns from alloys #2 (a) and #1 (b) cooled from 1400°C showing B2 order and <110> diffuse streaks. Specimens cooled from 1100°C are similar.

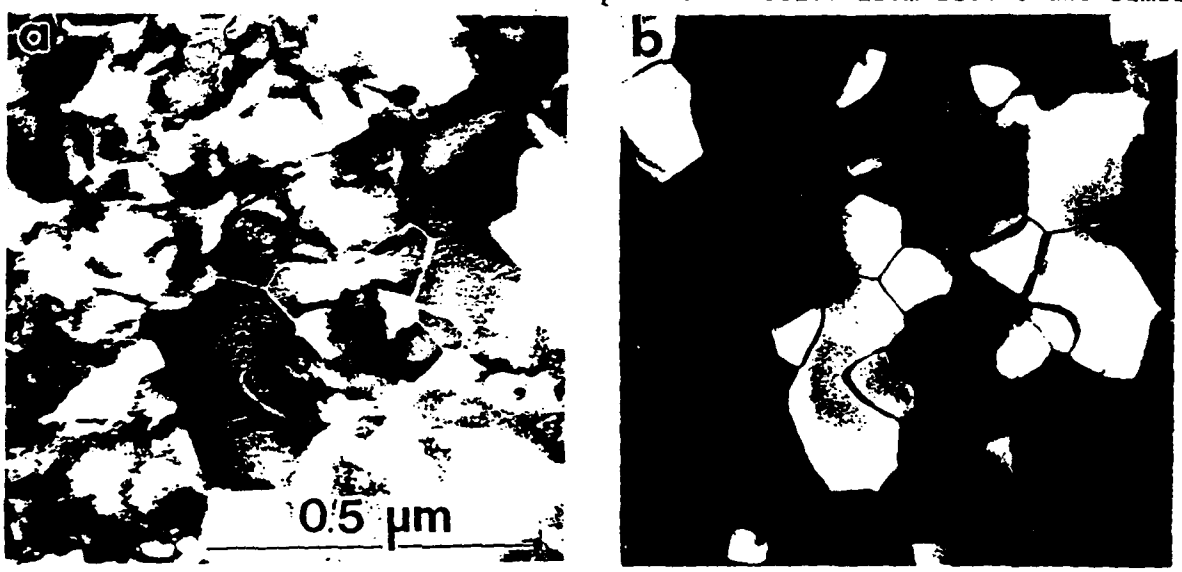

FIG.3 TEM bright-field (a) and dark-field (b) of #4 alloy cooled from 1400°C. Dark-field shows only one (out of four rotational domains of the omega-type phase. Interfaces within the domains separate translational domains.

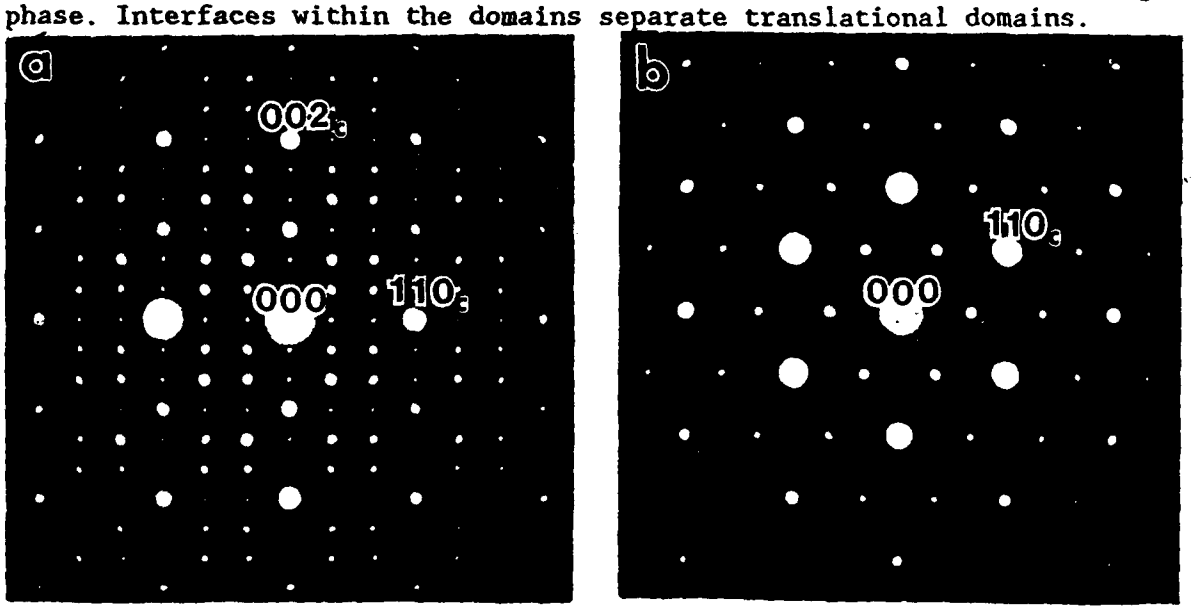

FIG.4 SADP patterns typical for the alloy #4 cooled from either 1400°C or 1100°C. a) $[110]_{bcc}$ zone axis; b) $[111]_{bcc}$ zone axis.

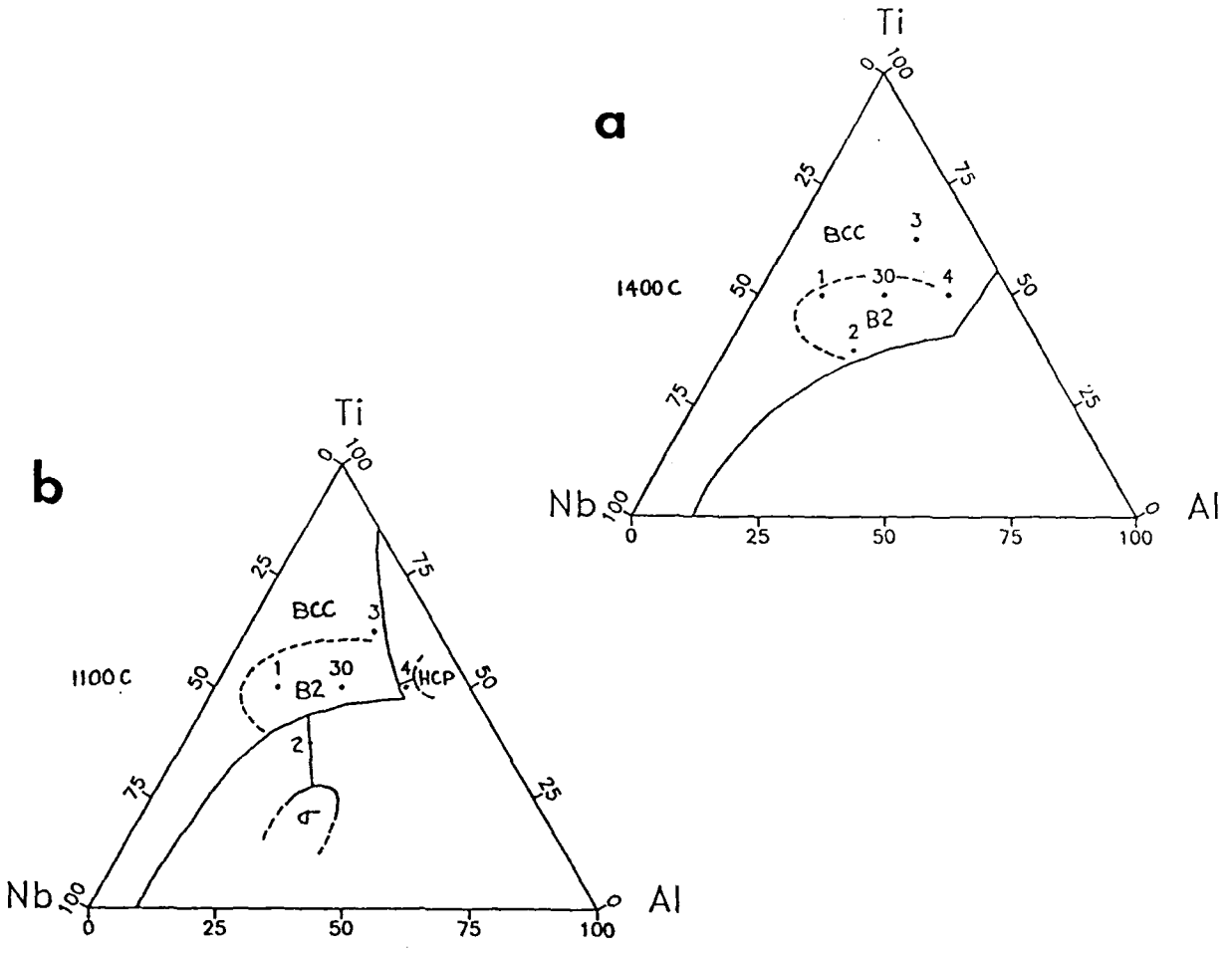

FIG.5 The estimated single phase field of the BCC phase at (a) 1400°C and (b) 1100°C. Dashed line shows a possible field where the BCC phase is ordered to B2. Tie lines to the sigma and hcp phases determined by microprobe are shown in (b).

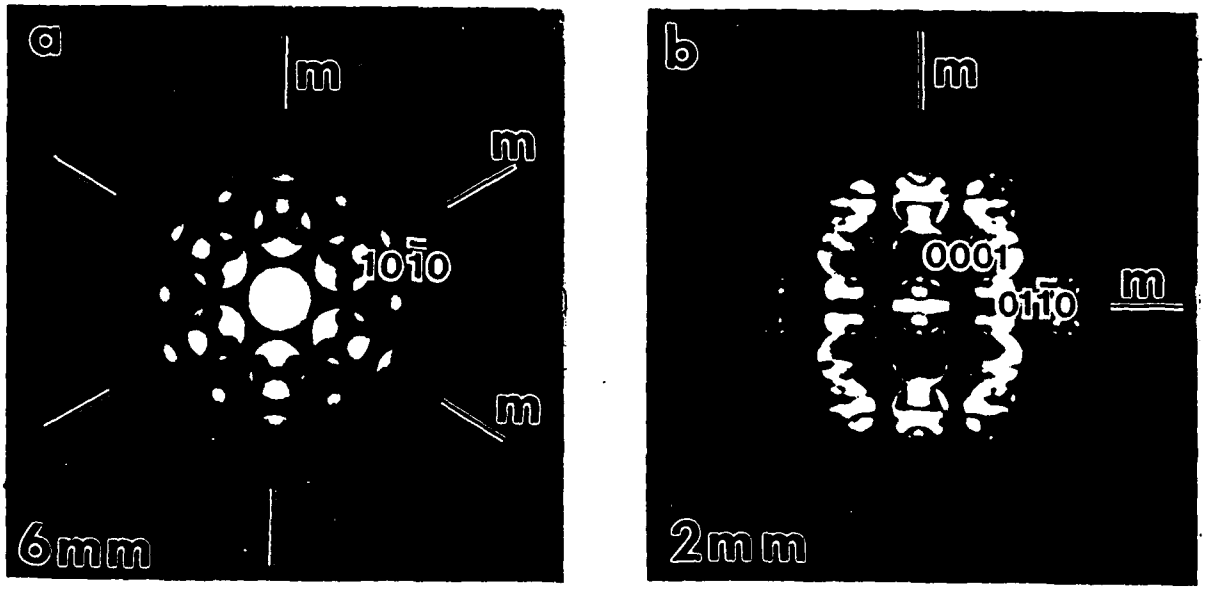

FIG.6 CBED from a single domain of alloy #4 anealed at 700°C for 26 days at [0001] (a) and [1120] (b) zone axis orientations showing 6mm and 2mm whole pattern symmetry consistent with the $P6_3/mmc$ space group of $B8_2$ structure.